SIAM J. Applied Dynamical Systems
Vol. 2, No. 2, pp. 187–218

A Simply Stabilized Running Model*

R. M. Ghigliazza†, R. Altendorfer‡, P. Holmes§, and D. Koditschek‡

Abstract. The spring-loaded inverted pendulum (SLIP), or monopedal hopper, is an archetypal model for running in numerous animal species. Although locomotion is generally considered a complex task requiring sophisticated control strategies to account for coordination and stability, we show that stable gaits can be found in the SLIP with both linear and "air" springs, controlled by a simple fixed-leg reset policy. We first derive touchdown-to-touchdown Poincaré maps under the common assumption of negligible gravitational effects during the stance phase. We subsequently include and assess these effects and briefly consider coupling to pitching motions. We investigate the domains of attraction of symmetric periodic gaits and bifurcations from the branches of stable gaits in terms of nondimensional parameters.

Key words. legged locomotion, spring-loaded inverted pendulum, periodic gaits, bifurcation, stability

AMS subject classifications. 34C23, 37J20, 37J25, 37J60, 70Hxx, 70K42, 70K50

PII. S1111111102408311

1. Introduction.

Locomotion, "moving the body's locus," is among the most fundamental of animal behaviors. A large motor science literature addresses gait pattern selection [1], energy expenditure [2], underlying neurophysiology [3], and coordination in animals and machines [4]. In this paper, we explore the stabilizing effect of a very simple control policy on a very simple running model.

Legged locomotion is generally considered a complex task [5] involving the coordination of many limbs and redundant degrees of freedom [6]. In [7], Full and Koditschek note that "locomotion results from complex, high-dimensional, non-linear, dynamically coupled interactions between an organism and its environment." They distinguish locomotion models simplified for the purpose of task specification (templates) from more kinematically and dynamically accurate representations of the true body morphology (anchors). A *template* is a formal reductive model that (1) encodes parsimoniously the dynamics of the body and its payload transport capability, using the minimum number of variables and parameters, and (2) advances an intrinsic hypothesis concerning the control strategy underlying the achievement of this task. *Anchors* are not only more elaborate dynamical systems grounded in the morphology and physiology

*Received by the editors May 23, 2002; accepted for publication (in revised form) by M. Golubitsky January 29, 2003; published electronically May 8, 2003. This work was supported by DoE grant DE-FG02-95ER25238 and DARPA/ONR grant N00014-98-1-0747.
http://www.siam.org/journals/siads/2-2/40831.html
†Department of Mechanical and Aerospace Engineering, Princeton University, Princeton, NJ 08544 (rghiglia@princeton.edu). This author was partially supported by Burroughs-Wellcome Training Grant in Biological Dynamics 1001782.
‡Department of Electrical Engineering and Computer Science, University of Michigan, Ann Arbor, MI 48109 (altendor@eecs.umich.edu, kod@umich.edu).
§Department of Mechanical and Aerospace Engineering, Program in Applied and Computational Mathematics, Princeton University, Princeton, NJ 08544 (pholmes@math.princeton.edu).

of an animal, but they must also admit the imposition of control policies that result in the realization of the lower dimensional template dynamics. In this context, Full and Koditschek suggest that the spring-loaded inverted pendulum (SLIP) model might reasonably provide a template for sagittal plane motions of the center of mass (COM) of such diverse species as six-legged trotters (cockroaches), four-legged trotters (dogs), two-legged runners (humans and birds), and hoppers (kangaroos). The validation of the SLIP template is based on similarities of ground reaction forces and kinetic and potential energies between these animals running at steady state and the SLIP model with suitably adjusted parameters (see [8]; for a review, see [9]). Details of the anchor system such as pitching motion or multiple leg impacts lead to small deviations from the SLIP predictions, which can be quantified by a more detailed error analysis (see [10] and the references therein).

In related work, McGeer [11] and, more recently, Ruina and colleagues [12, 13] have designed, analyzed, and built passive walking machines that are entirely uncontrolled yet produce stable gaits. These differ from SLIP-type machines in that their rigid legs incur impacts at touchdown, and stable gaits emerge from a balance between energy supplied by motion down an inclined plane and energy losses due to impacts. Their mathematical models are significantly more complicated than the SLIP, and only limited analyses are possible. Similarly, a recent study of Mombaur et al. [14] relies on numerical optimization methods to find the "most stable" periodic gaits of a four-degree-of-freedom hopper endowed with a massy leg and a circular foot. They apply feedforward actuation via programmable leg length and hip torque and note that damper forces and impact losses "may promote stability." In contrast, the SLIP machines investigated in this paper are conservative and operate at constant energy; no friction forces are present, and no impact occurs at touchdown (see section 2 for details of the model).

Models as simple and (relatively) analytically tractable as the SLIP can address two key questions: how much energy and how much information are needed to sustain a gait? With regard to the second question, many researchers (e.g., [4, 15, 6]) implicitly assume that even if "passive dynamic" periodic gaits exist, they are (highly [4]) unstable. A surprising answer to both questions, motivated by hypotheses proposed in [16], was found by Schmitt and Holmes [17, 18, 19, 20] for the mechanics of a lateral leg spring (LLS) model (essentially a SLIP without gravity or flight phases), which describes horizontal plane motions of a rigid body equipped with a pair of massless springy legs that are lifted when leg force drops to zero, are swung forward, and are set down at fixed angles relative to the body. They showed that, even without energy dissipation, the LLS model can exhibit stable periodic gaits. Liftoff events alone trigger the swing phases: continuous (neural) sensing is not required, and stability derives from angular momentum trading from step to step. Moreover, recent experiments [21] have suggested that rapidly running insects do employ such mechanical reaction forces to make heading corrections.

In this paper, we demonstrate and, under simplifying assumptions, prove that stable periodic gaits exist in very simply controlled SLIP models over a physically useful range of parameter values. Specifically, we show that a liftoff-event-triggered reset of the leg angle during flight to achieve a touchdown angle fixed at the same value for each stance phase (hereafter, *fixed-leg reset*) suffices for stability. Such self-stabilized SLIP gaits have already appeared in the literature [10, Figure 2], where periodic SLIP trajectories were compared to

experimental data, although their stability properties were not discussed. Our present work also complements a recent paper of Seyfarth et al. [22], in which parameter ranges for stable, symmetric, periodic SLIP gaits are found by numerical simulation and are compared with data from human running. Here we derive analytical results, perform detailed bifurcation and parameter studies (including a second, nonlinear spring model), explain mechanisms responsible for stable gaits, and elucidate limits to fixed-leg reset stability. We relate our results to [22] where appropriate and summarize the relationship between that and the present work in section 5.

Our main results may be summarized as follows. Using conservation laws and simple geometric relations, we produce closed form approximations (explicit up to the evaluation of a quadrature integral) for the touchdown-to-touchdown Poincaré map and the "stability eigenvalue" of its fixed point for a simplified version of the model; see (2.20), (2.24), and Figures 7 and 11. These allow us to plot branches of stable and unstable periodic gaits (Figures 8 and 13) and to understand how the domains of attraction of the stable gaits depend upon parameters. Particular spring laws appear only in the quadrature. We believe that such explicit approximations have not previously appeared; moreover, exact Poincaré maps, requiring only numerical evaluation of the leg sweep angle during stance, are implicit in our derivation. An appropriate notion of stability for such piecewise-holonomic systems [23] is that of *partial asymptotic stability*. Due to energy conservation and rotational invariance (in the case of coincident "hip joint" and mass center), one or three of the eigenvalues of the linearized Poincaré map are necessarily unity, leaving a single "stability eigenvalue" that may lie within or outside the unit circle. Thus, at best, the orbits are only Liapunov or neutrally stable.

The paper is organized as follows. In section 2, we set up the general rigid body model and then focus on an integrable case, in which pitching motions decouple and gravity is neglected during the stance phase (2.1). This allows us to derive explicit stride-to-stride (Poincaré) maps and obtain expressions characterizing periodic gaits, their stability, and bifurcations. Apart from illustrations, this is all done for general leg-spring laws. We then give convincing numerical evidence that stable gaits persist under the inclusion of gravity during stance (2.2) and under coupling to pitching motions (2.3). In section 3, we illustrate our results using the classical Hooke's law spring (3.1) and a progressively hardening compressed air spring (3.2). In section 4, we reformulate the equations of motion in nondimensional variables and include gravity during stance, thereby clarifying the effects of parameter variations and the resulting range of behaviors exhibited by the model. Finally, section 5 summarizes the work and notes possible extensions.

This work has two main goals: to better understand animal locomotion and to stimulate and enable the creation of "bio-inspired" robots. A significant part of locomotion research is driven by the desire to exploit the advantages of legged robots as opposed to wheeled and tracked vehicles. Nature suggests (and engineers are increasingly concerned to demonstrate) that legged robots can operate over a greater range of environmental and surface conditions, combining dexterity with mobility and efficiency; cf. [24, 10]. In addition, machines that use ballistic flight phases do not require continuous support paths [5].

A natural extension of the work presented here is the design of control algorithms that enlarge the rather small basin of attraction of the SLIP with a constant leg touchdown angle

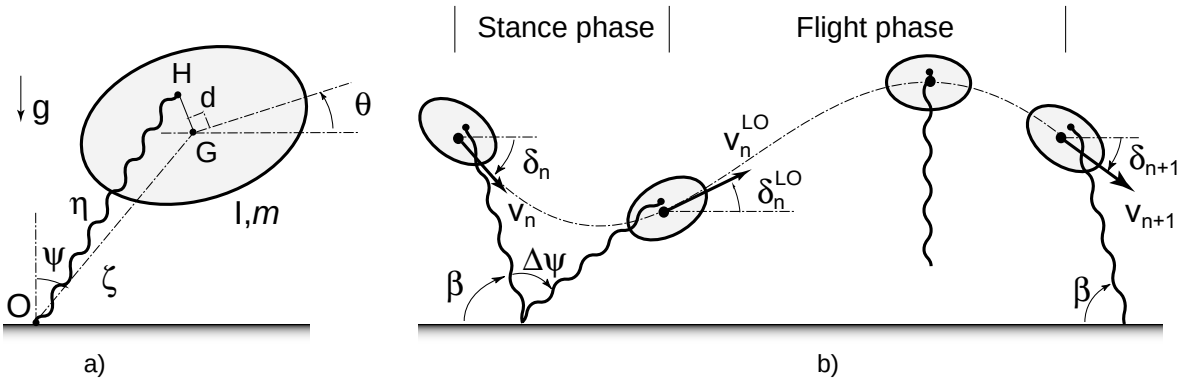

Figure 1. *The hopping rigid body* (a)*, and the stance and flight phases comprising a full stride* (b).

control [25]. A globally attracting "low attention" feedback controller was proposed in [26] by making the leg angle trajectory time-dependent during flight. However, this controller was based on a numerically precomputed leg trajectory and required velocity sensing. This raises the question of how much sensing is required to obtain "large" basins of attraction. A first step in this direction was undertaken in [27], where a necessary condition for the stability of fixed points for arbitrary leg angle trajectories was formulated in terms of the sensor requirements at liftoff. We will further explore this issue in a forthcoming paper [28]. Control enters the present paper only as the fixed feedforward leg placement strategy used at touchdown to define the hybrid switching condition.

2. The model: Equations of motion. Figure 1(a) illustrates our parametrization of the SLIP model as a schematic representation for the stance phase of a running (or hopping) biped with at most one foot on the ground at any time. This model incorporates a rigid body of mass m and moment of inertia I, possessing a massless sprung leg attached at a hip joint, H, a distance d from the COM, G. The figure depicts the attitude or pitch angle θ, the angle ψ formed between the line joining foothold O to the COM and the vertical (gravity) axis, and the distance ζ from foothold to the COM. The quantity

$$\eta = \sqrt{d^2 + \zeta^2 + 2d\zeta\cos(\psi + \theta)} \tag{2.1}$$

measures the (compressed) leg-spring length: the distance between O and the hip pivot H. We take frictionless pin joints at O and H. The body is assumed to remain in the vertical (sagittal) plane, and its state at any point in time is defined by the position of G, (x_G, y_G) referred to a Cartesian inertial frame, and the pitch angle θ; during stance we will also use the generalized polar coordinates ζ, ψ, based at the foothold O, and θ. (Note that ψ increases clockwise, while θ increases counterclockwise.) Unlike many earlier studies of the SLIP, we consider a rigid body with distributed mass and allow pitching motions,[1] although in the present paper we focus our attention upon the uncoupled case $d = 0$ and assume $\theta \equiv 0$, thus largely restricting ourselves to the point mass case.

[1] A bipedal walker with the above-described leg and body geometry with arbitrary radial force in the leg and arbitrary hip torque was considered in [29] in the context of feedback control. However, the investigation did not include gaits with flight phases.

A full stride divides into a stance phase, with foothold O fixed, the leg under compression, and the body swinging forward (ψ increasing), and a flight phase in which the body describes a ballistic trajectory under the sole influence of gravity. The stance phase ends when the spring unloads; the flight phase then begins, continuing until touchdown, which occurs when the landing leg, uncompressed and set at a predetermined angle β, next contacts the ground. See Figure 1. This defines a *hybrid* system in which touchdown and liftoff conditions mark transitions between two dynamical régimes.

Recalling previous robotics research [30] and looking ahead to control studies [28], β could be adjusted from stride to stride (necessitating at least intermittent active neural feedback), but here it will be taken as a fixed parameter. The "fixed leg reset angle" policy of stated interest might be implemented with respect either to the body or to the inertial frame. In the first case, touchdown occurs when the hip reaches the height $\eta_0 \sin(\beta - \theta)$ and in the second case when the hip reaches the height $\eta_0 \sin\beta$. Liftoff occurs automatically when the spring force drops to zero, requiring no sensing, but in any physical implementation, even a fixed-leg reset policy requires some state information to initiate the swing phase (e.g., a contact sensor in the foot or force sensor in the spring).

The kinetic energy of the body is

$$T = \frac{1}{2}m(\dot{\zeta}^2 + \zeta^2\dot{\psi}^2) + \frac{1}{2}I\dot{\theta}^2, \tag{2.2}$$

and its potential energy is

$$V_{tot} = mg\zeta\cos\psi + V\left(\eta\left(\zeta,\psi,\theta\right)\right), \tag{2.3}$$

where $V = V_{spr}$ denotes the spring potential. Forming the Lagrangian $L = T - V$ and writing $\partial V/\partial\eta = V_\eta$, we obtain the equations of motion for the stance phase:

$$\begin{aligned}
\ddot{\zeta} &= \zeta\dot{\psi}^2 - g\cos\psi - \frac{V_\eta\left(\eta\right)}{m\eta}\left(\zeta + d\cos\left(\psi+\theta\right)\right),\\
\zeta\ddot{\psi} &= -2\dot{\zeta}\dot{\psi} + g\sin\psi + d\frac{V_\eta\left(\eta\right)}{m\eta}\left(\sin\left(\psi+\theta\right)\right),\\
\ddot{\theta} &= d\zeta\frac{V_\eta(\eta)}{\eta I}\sin\left(\psi+\theta\right).
\end{aligned} \tag{2.4}$$

The equations of motion during the flight phase are simply the ballistic COM translation and torque-free rotation equations, which may be integrated to yield

$$x_G\left(t\right) = x^{LO} + \dot{x}^{LO}t, \quad y_G\left(t\right) = y^{LO} + \dot{y}^{LO}t - \frac{1}{2}gt^2, \quad \theta\left(t\right) = \theta^{LO} + \dot{\theta}^{LO}t, \tag{2.5}$$

where (x_G, y_G) denotes the COM position and θ the pitch angle, and the superscripts LO refer to the system state at liftoff.

2.1. The case $d = 0$ neglecting gravitational effects in stance. If the leg is attached at the COM ($H \equiv G$), then $d = 0, \zeta \equiv \eta$, the stance phase dynamics simplifies to the "classical"

SLIP, and the pitching equation decouples:

$$\ddot{\zeta} = \zeta\dot{\psi}^2 - g\cos\psi - \frac{V_\zeta(\zeta)}{m}\ , \quad \zeta\ddot{\psi} = -2\dot{\zeta}\dot{\psi} + g\sin\psi,$$
$$\ddot{\theta} = 0 \Rightarrow \theta(t) = \theta(0) + \dot{\theta}(0)\,t. \tag{2.6}$$

The third equation describes the conservation of angular momentum of the body about its COM: $I\dot{\theta} \triangleq p_\theta = \text{const}$.

Neglect of gravity in stance yields an integrable system [31]. A detailed analysis of the validity of this approximation for different spring potentials was performed in [32] using Hamiltonian instead of Lagrangian formalism. This simplification was shown to be too crude over a large range of running gaits, and several closed form approximations to the stance phase dynamics were proposed, although existence and stability of periodic solutions that can arise from concatenation of stance and flight phases were not investigated. Despite the limited accuracy of the gravity-free approximation, we adopt it here in order to gain an analytical understanding of periodic gaits. We will subsequently compare these results to numerical simulations of the full stance dynamics with gravity and show that analogous bifurcation structures persist in the physically more accurate model.

Neglecting gravity, the first two equations of (2.6) simplify to

$$\ddot{\zeta} = \zeta\dot{\psi}^2 - \frac{V_\zeta(\zeta)}{m}\ ,\ \zeta\ddot{\psi} = -2\dot{\zeta}\dot{\psi}. \tag{2.7}$$

The second of these equations expresses the conservation of the moment of linear momentum of the COM about the foot: $m\dot{\psi}\zeta^2 \triangleq p_\psi = \text{const}$. The first equation is, therefore, integrable:

$$\ddot{\zeta} = \frac{p_\psi^2}{m^2\zeta^3} - \frac{V_\zeta(\zeta)}{m} \ \Rightarrow\ m\ddot{\zeta}\dot{\zeta} = \frac{p_\psi^2}{m\zeta^3}\dot{\zeta} - V_\zeta(\zeta)\,\dot{\zeta} \ \Rightarrow$$
$$H \triangleq \left(\frac{m\dot{\zeta}^2}{2} + \frac{p_\psi^2}{2m\zeta^2} + V(\zeta)\right) = \text{const}. \tag{2.8}$$

Indeed, in the absence of dissipative forces, the total energy, which coincides here with the Hamiltonian $H = T+V = E$, is conserved. The original three degrees of freedom reduce to one due to the conservation of moment of linear momentum p_ψ and body angular momentum p_θ individually. The phase portrait during stance is then given by the level sets of H in the region $\zeta \le \eta_0$; Figure 2 illustrates this for a linear spring and also includes comparisons to solutions of the full system (2.6), including gravity. Three cases are shown, with different stiffness/gravity ratios characterized by the nondimensional parameter $\gamma = \frac{k\eta_0}{mg} \in [10, 100]$. As expected [33, 34], the integrable portraits are perturbed by the inclusion of gravity, but orbits retain the same qualitative characteristics. Leg stiffnesses estimated for human running, for example, give $\gamma \in (10, 21)$ [35, 36] (although Seyfarth et al. propose significantly higher values ($\gamma \in (25, 70)$; cf. [22, Fig. 2A]). Errors approach 20% at the lower end of this range at midstance (near $\dot{\zeta} = 0$ in Figure 2(c)) but are smaller at liftoff. Extensive simulation experience confirms that errors decrease with increasing γ (or k) for initial conditions away from the extremes of the physically interesting operating regimes; see [32] for a careful discussion of such modeling errors; also see

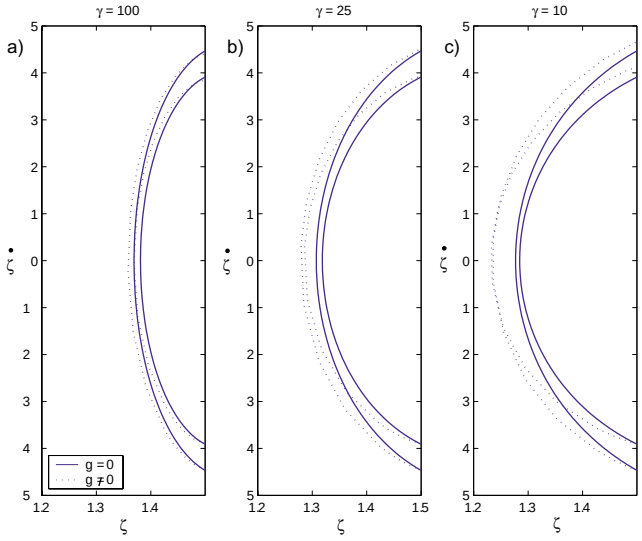

Figure 2. *Solutions of the integrable system (2.7) (solid) and the full ($d = 0$) system (dashed) in the stance phase: $m = 1, \eta_0 = 1.5, \beta = \pi/4$ with linear spring stiffnesses $k = 654$ ($\gamma = 100$) (a), $k = 163.5$ ($\gamma = 25$) (b), and $k = 65.4$ ($\gamma = 10$) (c). Dimensional units, unless otherwise stated, are MKS.*

section 2.2 and Figure 4 below. Moreover, for orbits reflection-symmetric about midstance for which $\psi(t)$ is an odd function, such as the periodic gaits to be found below, the net angular impulse delivered during each stance phase is zero so that, while p_ψ is not conserved, it does regain its touchdown value at liftoff. This also tends to minimize errors.

In principle, we can integrate (2.8), first solving for time in terms of ζ and then inverting and solving for $\zeta(t)$ and $\psi(t)$. In particular, the quadrature determining the angle swept by the leg may be written as $\Delta\psi(v_n, \delta_n) = \int_0^\tau \frac{p_\psi}{m\zeta^2} dt$, where v_n and δ_n denote the COM velocity magnitude and direction relative to horizontal at the nth touchdown instant. Hence the moment of linear momentum for the nth stance phase may be computed as $p_\psi = m\eta_0 v_n \sin(\beta - \delta_n)$. Then, from conservation of energy (2.8), we have

$$\dot{\zeta} = \sqrt{\frac{2}{m}\left(E - V(\zeta)\right) - \frac{p_\psi^2}{m^2\zeta^2}} \;\Rightarrow\; dt = \frac{m\, d\zeta}{\sqrt{2m\left(E - V\left(\zeta\right)\right) - \frac{p_\psi^2}{\zeta^2}}} \tag{2.9}$$

so that the sweep angle may then be expressed as the quadrature

$$\Delta\psi\left(v_n, \delta_n\right) = 2\int_{\zeta_b}^{\eta_0} \frac{\eta_0 v_n \sin(\beta - \delta_n)\, d\zeta}{\zeta^2\sqrt{v_n^2 - \frac{2V(\zeta)}{m} - \frac{\eta_0^2 v_n^2 sin^2(\beta - \delta_n)}{\zeta^2}}}. \tag{2.10}$$

Here we have set $E = \frac{1}{2}mv_n^2$, corresponding to the initial energy at touchdown, and $\zeta_b \le \eta_0$ denotes the midstride (compressed) leg length.

Computations of $\Delta\psi$ in specific cases of a linear spring and an "air spring" with potential $V(\eta) = \frac{c}{2}\left(\frac{1}{\eta} - \frac{1}{\eta_0}\right)^2$ are given in [17]. Schwind and Koditschek [32] develop an approximate

expression for this quadrature and compare it with both the exact integral and the analogous stance sweep angle including gravitational effects. In the present paper, we illustrate the general model again with a linear Hooke's law spring but adopt a different version of the nonlinear air spring model—specifically, that used in [37, 32]. While this potential, $V(\eta) = \frac{c}{2}(\frac{1}{\eta^2} - \frac{1}{\eta_0^2})$, results in an inverse cubic force law of the form $-\frac{c}{\eta^3}$ that is nonzero at touchdown and liftoff, energy is conserved since the leg lengths are the same ($\eta = \eta_0$), and velocities are continuous. The explicit sweep angle expression for this law is given in Appendix A. For the linear spring, $V(\zeta) = \frac{k}{2}(\eta - \eta_0)^2 = \frac{k}{2}(\zeta - \eta_0)^2$, and we have $\Delta\psi = \frac{2\sin(\beta-\delta)}{\sqrt{\tilde{k}}} D(\tilde{k}; \beta - \delta)$, where $\tilde{k} = \frac{k\eta_0^2}{mv_n^2}$ and the function $D(\tilde{k}; \beta - \delta)$ involves elliptic integrals [17, Appendix A.1.2].

The stance phase dynamics described above must be composed with the ballistic dynamics of the flight phase of (2.5), and the overall dynamics and the stability of this piecewise-holonomic system [31] are best described via Poincaré or return maps [34]. It is convenient to choose as generalized coordinates to describe the map the magnitude of touchdown and liftoff velocities v_n^{TD} and v_n^{LO}, respectively, and the relative angles δ_n^{TD} and δ_n^{LO} between the velocity vectors and the horizontal datum; see Figure 1b. The full map is obtained by composition of the stance phase map

$$P_{st} : \begin{bmatrix} v_n^{TD} \\ \delta_n^{TD} \end{bmatrix} \mapsto \begin{bmatrix} v_n^{LO} \\ \delta_n^{LO} \end{bmatrix} \tag{2.11}$$

and the flight map

$$P_{fl} : \begin{bmatrix} v_n^{LO} \\ \delta_n^{LO} \end{bmatrix} \mapsto \begin{bmatrix} v_{n+1}^{TD} \\ \delta_{n+1}^{TD} \end{bmatrix} \tag{2.12}$$

as

$$P = P_{fl} \circ P_{st} : \begin{bmatrix} v_n^{TD} \\ \delta_n^{TD} \end{bmatrix} \mapsto \begin{bmatrix} v_{n+1}^{TD} \\ \delta_{n+1}^{TD} \end{bmatrix}. \tag{2.13}$$

Since $I\dot{\theta} = I\dot{\theta}_0 = \text{const}$ implies that $\theta(t) = \theta_0 + \dot{\theta}_0 t$, and at touchdown in the first protocol the leg is placed at a fixed angle relative to the body, to obtain "sensible" periodic gaits we henceforth assume $\dot{\theta} = \dot{\theta}_0 = 0$. In this case, since $d = 0$ and $\theta \equiv 0$, there is no distinction between the two leg placement protocols.

We now describe the maps in detail, deriving explicit formulae. We shall frequently drop the superscript TD and write $v_n^{TD} = v_n$ and $\delta_n^{TD} = \delta_n$, it being understood that $(v_n, \delta_n) \mapsto P(v_n, \delta_n)$ denotes the touchdown-to-touchdown map.

2.1.1. Stance phase map. The spring is fully extended and stores no potential energy at the beginning or the end of each stance phase. Choosing the reference height for zero gravitational energy at $y = \eta_0 \sin\beta$, the energy at touchdown is therefore purely kinetic, $E_n^{TD} = \frac{1}{2}m(v_n^{TD})^2$, while at liftoff the energy has in general a gravitational component, $E_n^{LO} = \frac{1}{2}m(v_n^{LO})^2 + mg\eta_0(\sin(\beta + \Delta\psi) - \sin\beta)$, the last term being positive, zero, or negative. Appealing to overall energy conservation $E_n^{LO} = E_n^{TD}$, the liftoff velocity is therefore

$$v_n^{LO} = \sqrt{v_n^2 + 2g\eta_0(\sin\beta - \sin(\beta + \Delta\psi))}. \tag{2.14}$$

As noted earlier, if the spring is sufficiently stiff so that gravity is negligible, the moment of linear momentum p_ψ is conserved throughout stance in what is effectively a central force

problem [31]: $p_\psi = m\,\underline{r}_n \times \underline{v}_n = m\,\underline{r}_n^{LO} \times \underline{v}_n^{LO}$. Since $|\underline{r}_n \times \underline{v}_n| = \eta_0 v_n \sin(\delta_n - \beta)$ and $|\underline{r}_n^{LO} \times \underline{v}_n^{LO}| = \eta_0 v_n^{LO} \sin(\delta_n^{LO} - \pi + \Delta\psi + \beta)$, we obtain

$$\delta_n^{LO} = \pi - \Delta\psi - \beta + \sin^{-1}\left(\frac{v_n}{v_n^{LO}}\sin(\delta_n - \beta)\right). \tag{2.15}$$

However, since gravity is ignored in the sweep angle computation of (2.10), for consistency we must also ignore it in assigning a liftoff velocity magnitude in (2.15) and set $v_n^{LO} = v_n$ so that (2.15) simplifies to

$$\delta_n^{LO} = \delta_n + \pi - \Delta\psi(v_n, \delta_n) - 2\beta, \tag{2.16}$$

as in the LLS computations of [17]. Thus the effects of gravity are included in computing liftoff velocity magnitude (2.14) but *not* in approximating liftoff velocity direction (2.16). This "mixed approximation" has the advantage of retaining global energy conservation. Equations (2.14)–(2.16), with (2.10), specify P_{st}. Note that (2.14), along with a (numerical) calculation of the leg sweep angle $\Delta\psi$ and the change in p_ψ due to gravitational moment, defines the exact stance phase map including gravity. We use this in section 4.

We note that p_ψ is reset on each touchdown and that this "trading" of angular momentum from stride to stride will be responsible for asymptotic stability; cf. [17].

2.1.2. Flight phase and overall Poincaré map P. Using similar arguments based on conservation of energy,

$$E_n^{LO} = \frac{1}{2}m(v_n^{LO})^2 + mg\eta_0\left(\sin(\beta + \Delta\psi) - \sin(\beta)\right) = E_{n+1}^{TD} = \frac{1}{2}m(v_{n+1}^{TD})^2,$$

and on conservation of linear momentum in the horizontal direction,

$$v_n^{LO}\cos(\delta_n^{LO}) = v_{n+1}^{TD}\cos(\delta_{n+1}^{TD}), \tag{2.17}$$

we find the flight phase map. For convenience, both maps are specified here:

$$P_{st}: \begin{bmatrix} v_n^{LO} \\ \delta_n^{LO} \end{bmatrix} = \begin{bmatrix} \sqrt{v_n^2 + 2g\eta_0\left(\sin\beta - \sin(\beta + \Delta\psi)\right)} \\ \delta_n + \pi - \Delta\psi - 2\beta \end{bmatrix}, \tag{2.18}$$

$$P_{fl}: \begin{bmatrix} v_{n+1} \\ \cos(\delta_{n+1}) \end{bmatrix} = \begin{bmatrix} \sqrt{(v_n^{LO})^2 + 2g\eta_0\left(\sin(\beta + \Delta\psi) - \sin\beta\right)} \\ \frac{v_n^{LO}}{v_n}\cos(\delta_n^{LO}) \end{bmatrix}. \tag{2.19}$$

The last equation should more properly read $v_{n+1}^{TD}\cos(\delta_{n+1}^{TD}) = v_n^{LO}\cos(\delta_n^{LO})$, but provided β and η_0 remain constant, conservation of energy enforces, without approximations, that $v_{n+1} = v_n$ because the energy at the beginning and the end of each full stance + flight stride is entirely kinetic. The flight map is only implicitly defined, and it is not evident that one can find an expression in terms of v_n^{LO}, δ_n^{LO} above, especially because $\Delta\psi = \Delta\psi(v_n, \delta_n)$ is a complicated function of the touchdown conditions; see (2.10). Nonetheless, using $v_{n+1} = v_n$, the full map simplifies considerably:

$$P: \begin{bmatrix} v_{n+1} \\ \cos(\delta_{n+1}) \end{bmatrix} = \begin{bmatrix} v_n \\ \sqrt{1 - \frac{2g\eta_0}{v_n^2}\left(\sin(\beta + \Delta\psi) - \sin\beta\right)}\cos(\delta_n + \pi - \Delta\psi - 2\beta) \end{bmatrix}. \tag{2.20}$$

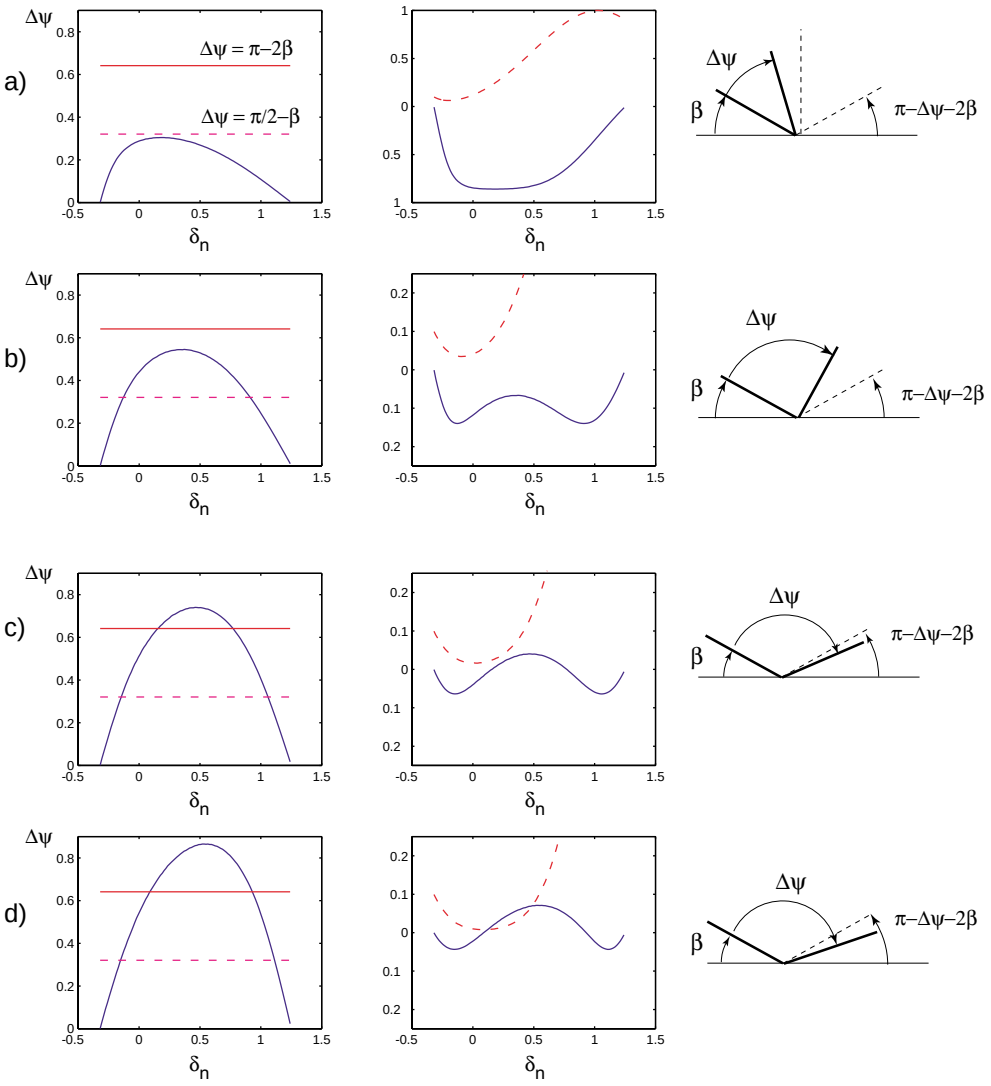

Figure 3. *The first column shows the function $\Delta\psi$ computed for a linear spring with $k = 100, m = 1, \eta_0 = 1.5$, and $\beta = 1.25$. For cases* (a) *through* (d)*, we set $\bar{v} = 1.75, 3.5, 5$, and 6, respectively. The conditions $\Delta\psi = \pi - 2\beta$ (dotted) and $\Delta\psi = \frac{\pi}{2} - \beta$ (dashed) are also shown. The second column shows the left-hand (dotted) and right-hand (solid) sides of inequality* (2.26)*: see sections* 2.1.4–2.1.5*. The third column shows β and $\Delta\psi$ in physical space: solid lines indicate angles at touchdown (β) and liftoff ($\beta + \Delta\psi$). When $\beta + \Delta\psi < \pi - \Delta\psi - 2\beta$ (cases* (a) *and* (b)*), the body leaves the ground at an angle closer to vertical than at touchdown. Note that* (2.26) *is violated for part of the domain in* (d)*.*

This expression is explicit apart from the sweep angle $\Delta\psi(v_n, \delta_n)$, which must be computed from the quadrature of (2.10). Only here does the specific spring potential enter; the rest of the expression for P is derived purely from conservation laws and stance and flight path geometry. Note that, although we have approximated $\Delta\psi$ and hence P_{st} by neglecting the

effect of gravitational torque in changing the COM angular momentum about the foot, the overall composed map P conserves energy, as would the exact solutions of (2.6).

We postpone quantitative analyses of specific spring potentials to sections 3–4; however, we note that analysis of special cases and numerical evidence indicates that for linear and stiffening springs, $\Delta\psi$ has a single maximum. This will suffice for the analysis of the present section. In particular, it is clear that for $\delta_n = \beta - \pi/2$ (glancing contact), $\tau = \Delta\psi = 0$, and for $\delta_n = \beta$ (running directly into the leg), $\Delta\psi = 0$. Thus $\Delta\psi = 0$ at both limits of the admissible δ range, while for any $v_n \neq 0$, $\Delta\psi > 0 \ \forall \ \delta_n \in (\beta - \pi/2, \beta)$, so there must be at least one maximum. We suspect that any physically reasonable spring law will give a $\Delta\psi$ with a unique maximum. The left column of Figure 3 shows $\Delta\psi$ for the linear spring evaluated numerically for several $\bar{v}$ values; they are indistinguishable from those obtained via the analytical expressions of [17].

We remark that, in view of energy conservation and the resulting constancy of v_n, (2.20) defines a one-dimensional map for the touchdown angle δ_n. One could specify the system's state in terms of any other convenient variable, such as the COM height at the apex, which was the choice adopted in [22]; cf. Figure 3(A) of that paper. We prefer to use the touchdown angle and retain the velocity as a second state variable so that, when $d \neq 0$, we may more conveniently couple in the attitude dynamics in terms of θ and $\dot{\theta}$, as was done for yawing motions in the LLS models of [17, 19]. Also, as demonstrated below, branches of periodic orbits and their domains of attraction are conveniently presented in terms of δ_n (cf. Figure 8).

2.1.3. Periodic gaits. The simplest sustained forward motions, in which the hopper maintains a constant average forward speed and lands with the same angle between the velocity vector and the horizontal datum on each step, are period one orbits given by $v_{n+1} = v_n$ and $\delta_{n+1} = \delta_n$. As we see from (2.20), the first condition is always satisfied, whereas the second condition holds if and only if $\Delta\psi\,(v_n, \delta_n) = \pi - 2\beta$.

To verify this, we first check sufficiency. Let $\Delta\psi(v_n, \delta_n) = \pi - 2\beta$. Then $\sin(\beta + \Delta\psi) - \sin\beta = \sin(\pi - \beta) - \sin\beta = 0$, and the map (2.20) reduces to

$$P : \begin{bmatrix} v_{n+1} \\ \cos(\delta_{n+1}) \end{bmatrix} = \begin{bmatrix} v_n \\ \cos(\delta_n) \end{bmatrix}. \tag{2.21}$$

At touchdown following a flight phase, $\delta_n \in [0, \pi]$ (for both locomotion directions). In that range, $\cos\delta_n$ is invertible; hence $\delta_{n+1} = \delta_n$.

Now let $\delta_{n+1} = \delta_n$. For sustained forward motion, $\Delta\psi(v_n, \delta_n) \in [\pi/2 - \beta, \pi - \beta]$ and $\delta_n^{LO} \in [0, \pi/2]$. Assume $\Delta\psi(v_n, \delta_n) > \pi - 2\beta$. Then $\delta_n^{LO} = \delta_n + \pi - \Delta\psi - 2\beta < \delta_n$ and $\cos\delta_n^{LO} > \cos\delta_n \ \forall \delta_n, \delta_n^{LO} \in [0, \pi/2]$. Also, $\beta + \Delta\psi > \pi - \beta$ and $\sin(\beta + \Delta\psi) < \sin(\pi - \beta)$ $\forall \beta \in [0, \pi/2]$ and $\forall \Delta\psi \in [\pi/2 - \beta, \pi - \beta] \Rightarrow \sin(\beta + \Delta\psi) - \sin\beta < 0 \ \forall \beta \in [0, \pi/2]$. Hence we conclude that

$$\cos(\delta_{n+1}) > \left[1 - \frac{2g\eta_0}{v_n^2}\left(\sin(\beta + \Delta\psi) - \sin\beta\right)\right]^{\frac{1}{2}} \cos(\delta_n) > \cos(\delta_n), \tag{2.22}$$

which is a contradiction. A similar argument holds for $\Delta\psi(v_n, \delta_n) < \pi - 2\beta$. Therefore, $\Delta\psi(v_n, \delta_n) = \pi - 2\beta$ is also necessary. Hence $\delta_n^{LO} = \delta_n$, and in the gravity-free approximation with $d = 0$, all one-periodic gaits are reflection-symmetric about midstance [38].

Note that, within limits to be determined below, $v_{n+1} = v_n = \bar{v}$ can be chosen arbitrarily, and the expression $\Delta\psi(\bar{v}, \delta_n) = \pi - 2\beta$ can be solved to obtain the fixed point that we denote by $\bar{\delta}$. Here we appeal to the fact that a parabolic segment of the flight trajectory can always be matched to connect reflection-symmetric stance phases (i.e., those having $\delta_n^{LO} = \delta_n$; see Figure 1), yielding a fixed point of P. Thus, there is a one-parameter ($\bar{v}$-) family of steady periodic gaits for each β and all other parameters fixed. Also see [17] and Figure 8.

We may linearize the general expression (2.20) at a fixed point of the map to obtain the Jacobian matrix

$$DP|_{\delta_n=\bar{\delta}} = \left[\begin{array}{cc} 1 & 0 \\ -\left(1 + \frac{g\eta_0 \cos\beta \cot\delta_n}{\bar{v}^2}\right) & 1 - \left(1 + \frac{g\eta_0 \cos\beta \cot\delta_n}{\bar{v}^2}\right)\frac{\partial\Delta\psi}{\partial\delta_n} \end{array} \right]\Bigg|_{\delta_n=\bar{\delta}}, \tag{2.23}$$

the eigenvalues of which are $\lambda_1 = 1$ and

$$\lambda_2 = 1 - \left(1 + \frac{g\eta_0 \cos\beta \cot\delta_n}{\bar{v}^2}\right)\frac{\partial\Delta\psi}{\partial\delta_n}\Bigg|_{\delta_n=\bar{\delta}}. \tag{2.24}$$

The first eigenvalue, λ_1, lies on the unit circle, corresponding to conservation of energy, but $|\lambda_2|$ may take values either greater than or less than 1. We require $\bar{\delta} \in (0, \beta)$ and $\beta \in \left(0, \frac{\pi}{2}\right)$ for physically admissible gaits; thus the quantity in parentheses in (2.24) is strictly positive, and a key factor in determining λ_2 is the sign of $\frac{\partial\Delta\psi}{\partial\delta_n}$. If $\frac{\partial\Delta\psi}{\partial\delta_n} < 0$, then $|\lambda_2| > 1$, and the fixed point is unstable; if $\frac{\partial\Delta\psi}{\partial\delta_n} > 0$, $|\lambda_2|$ may be less than or greater than 1, and stability or instability may ensue [39, 34] (see below).

As in [17], recognizing that energy is conserved, stability can only be *partially asymptotic*, since perturbations in the direction of the eigenvector of λ_1 neither grow nor decay. As noted at the close of section 2.1.1, both here and in [17], the physical mechanism for stabilization appears to be the trading of angular momentum from stride to stride. As noted by Ruina [23] (cf. [40]), such piecewise-holonomic systems can yield asymptotic stability much like nonholonomically constrained conservative systems [41].

2.1.4. Domain of definition of P. We must recall that the map was derived under the tacit assumption that unimpeded leg motion is possible over the entirety of the configuration space of the kinematic model. This is not true in general, as the toe must not be allowed to penetrate the ground. The touchdown angle β is held constant, and since the spring has a fixed length at rest η_0, the hip height at touchdown is also fixed: $y^{TD} = \eta_0 \sin\beta$. For a gait to exist, this height must be reached during the flight phase, i.e., $y_{G\,\max} \geq \eta_0 \sin\beta$; otherwise, the hopper will "stumble." Integrating the ballistic equations (2.5), the time of flight to reach the apex is $t_{\max} = v_n^{LO} \sin\delta_n^{LO}/g$, and the maximum height is given by (2.5):

$$y_{G\,\max} = y_G(t_{\max}) = \eta_0 \sin(\beta + \Delta\psi) + \frac{(v_n^{LO} \sin\delta_n^{LO})^2}{2g}.$$

Hence the map P is defined if and only if

$$\sin^2\delta_n^{LO} \geq \frac{2g\eta_o(\sin\beta - \sin(\beta + \Delta\psi))}{v_n^2 + 2g\eta_0(\sin\beta - \sin(\beta + \Delta\psi))} \tag{2.25}$$

or, using (2.16),

$$\sin^2(\delta_n + \pi - \Delta\psi - 2\beta) \geq \frac{2g\eta_o(\sin\beta - \sin(\beta + \Delta\psi))}{v_n^2 + 2g\eta_0(\sin\beta - \sin(\beta + \Delta\psi))}. \tag{2.26}$$

Inequality (2.26), which may be implicitly written in the form

$$f(\bar{v}, \delta_n; \beta, \eta_0, g, m, V(\cdot)) \geq 0,$$

specifies the domain of definition of P (admissible values of $(\bar{v}, \delta_n)$) for each choice of physical parameters (β, η_0, g, m) and spring potential V. It appears difficult to give explicit bounds, but we observe that, when $\max \Delta\psi(\bar{v}, \delta_n) \geq \pi - 2\beta$ and reflection-symmetric stance paths with $\delta_n = \bar{\delta}$ exist, we have $\sin(\beta + \Delta\psi) = \sin(\pi - \beta)$, and the right-hand side of (2.26) vanishes. For physically relevant gaits, $\bar{\delta} \in [0, \beta]$ and $\beta < \frac{\pi}{2}$; hence the left-hand side is strictly positive at fixed points unless $\bar{\delta} = 0$. However, since the spring remains compressed during stance, providing a positive radial force, we see that $\frac{d^2\zeta}{d\psi^2} > 0$, which implies $\frac{d^2\hat{y}}{d\hat{x}^2} > 0$, where $\hat{x}$ and $\hat{y}$ are the axes of a rotated orthogonal coordinate system that has its $\hat{y}$-axis aligned with the symmetry axis of the COM path. Hence the COM path is convex (cf. Figure 1), and $\bar{\delta} = 0$ cannot be a fixed point. (The COM path need not be convex when gravity is included; indeed, one may find orbits with $\delta_n^{TD} < 0$.) The second column of Figure 3 shows the two sides of inequality (2.26).

We may therefore conclude via continuous dependence on initial data that the domain of definition of P contains open sets around each fixed point, and, if $|\lambda_2| < 1$ (resp., > 1), local asymptotic stability (resp., instability) holds in the usual sense.

2.1.5. Bifurcations and stability of fixed points of P. To introduce the range of dynamical behaviors of P and better understand its domain of definition, we consider four representative cases depending on the maximum sweep angle $\Delta\psi_{\max}$:

(a) $\Delta\psi_{\max} < \frac{\pi}{2} - \beta$;
(b) $\frac{\pi}{2} - \beta < \Delta\psi_{\max} < \pi - 2\beta$;
(c) $\pi - 2\beta < \Delta\psi_{\max}$ and (2.26) is satisfied everywhere;
(d) $\pi - 2\beta < \Delta\psi_{\max}$ and (2.26) is not satisfied everywhere.

When $\Delta\psi_{\max} \leq \pi/2 - \beta$, the leg is vertical or directed forward at liftoff, so $\delta_{n+1}^{LO} > \delta_n$ and the direction of locomotion reverses once $\delta_n^{LO} > \pi/2$, even though the map may be well defined; see Figures 3(a) and 6(a).

For $\pi/2 - \beta < \Delta\psi_{\max} < \pi - 2\beta$, a domain appears in which $\psi_n^{LO} = \psi_n^{TD} + \Delta\psi_{\max} > 0$ and continuing forward motion is possible. However, the hopper still lifts off and touches down "more vertically" on each step until it eventually bounces backward in this case, too; see Figures 3(b) and 6(b). Indeed, from (2.16) we have $\delta_n^{LO} = \delta_n + \pi - \Delta\psi - 2\beta$, and by assumption (b) $\delta_n^{LO} > \delta_n$. From (2.17) we know that $\cos(\delta_{n+1}) = \frac{v_n^{LO}}{v_n}\cos(\delta_n^{LO})$. Now $\delta_n^{LO} \in \left(0, \frac{\pi}{2}\right)$, and the cosine function is monotonically decreasing. Since the hip position at liftoff is higher than at touchdown, the body has gained gravitational energy at the expense of kinetic energy. This means that $v_n^{LO} < v_n$, and therefore $\cos\delta_{n+1} = \frac{v_n^{LO}}{v_n}\cos\delta_n^{LO} < \cos\delta_n^{LO} < \cos\delta_n$. However, this implies that $\delta_{n+1} > \delta_n$. Thus, starting with an initial angle δ_n, after the stance phase, $\delta_n^{LO} > \delta_n$, and after the flight phase, $\delta_{n+1} > \delta_n^{LO} > \delta_n$. Hence succeeding touchdown angles

increase until progress is reversed; the dynamics is globally unstable, and the Poincaré map has no fixed points.

Cases (c) and (d) are of greater physical interest. In (c), inequality (2.26) is satisfied everywhere, so the domain of definition covers the interval $[\beta - \pi/2, \beta]$. Moreover, two fixed points exist, one of which may be stable, while the other (with higher values of $\bar{\delta}$) is unstable. These fixed points appear in a saddle-node bifurcation [34] at a critical speed $v = v_{SN}$. Indeed, for the smaller $\bar{\delta}$ fixed point, $\frac{\partial \Delta\psi}{\partial \delta_n} > 0$ (see Figure 3(c)), $\bar{\delta} > 0 \Rightarrow \cot\bar{\delta} > 0$, and $\lambda_2 = 1 - (1 + \frac{g\eta_0 \cos\beta \cot\bar{\delta}}{\bar{v}^2})\frac{\partial \Delta\psi}{\partial \delta_n} \stackrel{\triangle}{=} 1 - a\frac{\partial \Delta\psi}{\partial \delta_n}$. For the parameter values chosen here, $a \approx 3 > 0$; thus for $\frac{\partial \Delta\psi}{\partial \delta_n} \in (0, \frac{2}{3})$, $-1 < \lambda_2 < 1$, and we have established asymptotic stability. More generally, since the term $\frac{\partial \Delta\psi}{\partial \delta_n} = 0$ when $\Delta\psi_{\max} = \pi - 2\beta$, by continuous dependence on parameters $\frac{\partial \Delta\psi}{\partial \delta_n}$ is necessarily arbitrarily small for nearby parameter values, implying stability of the fixed point with smaller $\bar{\delta}$ in a neighborhood of the saddle-node bifurcation point. See Figures 3(c) and 6(c).

In case (d), $\Delta\psi_{max} \geq \pi - 2\beta$, but the map P is not everywhere defined: Figure 3(d) shows that inequality (2.26) fails in the interior of $[\beta - \pi/2, \beta]$. A *gap* opens between the fixed points and while a (stable) fixed point still exists to the left of the gap, many orbits, including that shown in Figure 6(d), enter the gap and "stumble."

We now summarize key aspects of the behaviors described above. More detailed analyses for specific spring potentials are given in sections 3–4.

Saddle-node bifurcation. As noted above, a saddle-node bifurcation occurs between regimes (b) and (c). Specifically, for parameter values such that

$$\Delta\psi_{\max}\left(\bar{v}_{SN}, \bar{\delta}_{SN}\right) = \pi - 2\beta \text{ and } \left.\frac{\partial \Delta\psi}{\partial \delta_n}\right|_{\left(\bar{v}_{SN}, \bar{\delta}_{SN}\right)} = 0, \tag{2.27}$$

the fixed points coalesce, and $\lambda_2 = 1$. For fixed physical parameters and $\bar{v} < \bar{v}_{SN}$, no fixed points exist, and periodic gaits are impossible; for a (possibly small) range of velocities $v > \bar{v}_{SN}$, a stable fixed point exists, corresponding to symmetric one-periodic gaits. See Figures 7 and 11.

Gaps. Increases in $\bar{v}$ and the consequent increases in the sweep angle $\Delta\psi_{\max}$ lead to a violation of (2.26), giving birth at a second critical speed $\bar{v} = \bar{v}_{GP}$ to a gap—an interior domain in which the map is not defined. With further increases in $\bar{v}$, the gap progressively expands to occupy a larger interval between the fixed points; see, e.g., Figure 8. Gaps may also appear in the range $\delta_n < 0$ for values of $\bar{v}$ small enough that $\Delta\psi_{\max} < \pi - 2\beta$, although these are of less physical importance, since sustained gaits do not exist in this range (below $\bar{v}_{SN}$). See the discussion of section 3.1 and Figure 7.

Period doubling. We recall expression (2.24) for the second eigenvalue of DP:

$$\lambda_2 = 1 - \left(1 + \frac{g\eta_0 \cos\beta \cot\delta_n}{\bar{v}^2}\right) \left.\frac{\partial \Delta\psi}{\partial \delta_n}\right|_{\delta_n \equiv \bar{\delta}}. \tag{2.28}$$

The quantity in parentheses is strictly positive for $\delta_n = \bar{\delta} \in (0, \beta)$ (symmetric periodic gaits), and $\frac{\partial \Delta\psi}{\partial \delta_n}|_{\delta_n = \bar{\delta}}$ is zero at the saddle-node bifurcation at $\bar{v} = \bar{v}_{SN}$ and thereafter positive at the stable fixed point of P. This suggests that, as the magnitude of $\frac{\partial \Delta\psi}{\partial \delta_n}|_{\delta_n = \bar{\delta}}$ increases with

increasing $\bar{v}$, λ_2 may pass through -1. For general (differentiable) maps, the instability arising from crossing the unit circle at $\lambda_2 = -1$ represents a loss of stability via period-doubling and the birth of a period two orbit [34].

Explicit computations are awkward due to the difficulty of evaluating the sweep angle quadrature (2.10), but we may estimate λ_2 and hence obtain a sufficient condition for period-doubling to occur at high velocities $\bar{v}$ by appealing to the limiting behavior of the $\Delta\psi$ as $\bar{v} \to \infty$. In the next section and in Appendix B, we estimate $\Delta\psi(\bar{v}, \delta_n)$ and the fixed-point location $\delta_n = \bar{\delta}$ in terms of the small parameter $\frac{1}{\bar{v}}$. This permits us to calculate $\frac{\partial \Delta\psi}{\partial \delta_n}|_{f.p.}$ in this limit, which in turn yields the estimate

$$\lambda_2 = -1 - \frac{\eta_0 \cos\beta\,[4mg + V'(\eta_0 \sin\beta)]}{\bar{v}\sqrt{2mV(\eta_0 \sin\beta)}} + \mathcal{O}\left(\frac{1}{\bar{v}^2}\right). \tag{2.29}$$

Since $V(\eta)$ is decreasing on the interval $(0, \eta_0)$ for physically reasonable spring laws, the condition $\lambda_2 = -1$ can indeed be met. Indeed, to guarantee it, bearing in mind the fact that for "low" $\bar{v} = \bar{v}_{SN}$, $\lambda_2 = +1$, it suffices to require $[4mg + V'(\eta_0 \sin\beta)] > 0$ so that λ_2 approaches -1 from below as $\bar{v} \to \infty$, having previously passed down through -1. Thus one would expect period-doubling to occur for relatively soft springs or touchdown angles close to 90^o, e.g., for $k\eta_0(1 - \sin\beta) < 4mg$ in the case of the linear spring of section 3.1. However, we recall that the approximate computation of the sweep angle employed in this section is carried out under the assumption that spring forces dominate gravitational effects, whereas (2.29) indicates that they should be comparable for period-doubling. Evidently, the true behavior of λ_2 depends in a subtle manner on the precise spring law and the other physical parameters.

Nonetheless, numerical evidence suggests that period-doubling does occur for reasonable parameter values and, moreover, that it can occur at relatively low speeds. This observation corrects the misleading claim in [22]: "Bistable solutions do not exist as only symmetric contact phases may result in a periodic movement pattern (Schwind, 1998)," and "More recently, Schwind (1998) showed that for a running spring-mass system only symmetric stance phases with respect to the vertical axis might result in cyclic movement trajectories."[2] Figure 9 shows an example of an attracting period two orbit born in such a bifurcation. Also see section 3.2. We remark that we have not found period-doubling for the Hooke spring with gravity in stance, since whenever we observe $\lambda_2 \leq -1$, the gap has already opened, which destroys any attracting behavior (see also Figure 3(A) of [22], where the gap opens at $\alpha_0 = 68.70^\circ$, whereas the slope of the left fixed point becomes -1 at $\alpha_0 = 68.85^\circ$).

We note that this behavior is markedly different from the LLS dynamics discussed in [17, 19], in which no flight phase occurs, and the bound $\frac{\partial \Delta\psi}{\partial \delta_n} < 2$ (see section 2.1.6) implies that period-doubling cannot occur.

2.1.6. The limiting case $\bar{v} \to \infty$. It was noted in [17] that there is a critical value $\bar{v}$ above which the touchdown kinetic energy exceeds the potential energy stored by a linear spring at zero length. When this happens, $\Delta\psi(\bar{v}, \delta_n)$ no longer has a quadratic shape but approaches

[2]The reader should note that the symmetry of orbits associated with period 1 return maps [36] has no bearing on the existence or properties of higher period discrete time behavior.

the straight line: $\Delta\psi = \pi - 2(\beta - \delta)$ as $\bar{v} \to \infty$. The unstable fixed point is lost, and the (previously stable) fixed point $\delta \to 0^+$, as shown in Figures 7 and 8. (As we shall see, this "change of type" does not occur for the air spring model, which has the physically desirable property that the spring force increases without bound as it is compressed to zero length.) However, for sufficiently large $\bar{v}$ and *any* spring law having bounded energy at nonzero length, kinetic energy dominates both gravitational and elastic energy at finite compression, and the COM follows an almost-straight "ballistic" horizontal path.

In this limit, the quadrature integral of (2.10) can be asymptotically estimated, as shown in Appendix B, leading to the following sweep angle expression:

$$\Delta\psi(\bar{v}, \delta_n) = (\pi - 2\beta + 2\delta_n) - \frac{1}{\bar{v}}\sqrt{\frac{2V(\eta_0 \sin(\beta - \delta_n))}{m}} + \mathcal{O}\left(\frac{1}{\bar{v}^2}\right). \tag{2.30}$$

This allows us to determine the limiting trajectory in physical space. Clearly the stance phase limits to a horizontal motion over the distance $2\eta_0 \cos\beta$ (the top of an inverted isosceles triangle). To compute the flight phase, we note that the fixed-point condition specifies $\Delta\psi(\bar{v}, \bar{\delta}) = \pi - 2\beta$. Calculating $\bar{\delta} \sim \frac{1}{\bar{v}}$ from the $\mathcal{O}(\frac{1}{\bar{v}})$ term of (2.30) (see Appendix B), we obtain an $\mathcal{O}(1)$ vertical component of liftoff velocity:

$$v^{LO}_{\text{vert}} = \bar{v}\sin\bar{\delta} \approx \sqrt{\frac{V(\eta_0 \sin\beta)}{2m}}\ ;\ v^{LO}_{\text{horiz}} = \bar{v}\cos\bar{\delta} \approx \bar{v}. \tag{2.31}$$

Hence the flight duration approaches a constant, and the flight distance grows linearly with $\bar{v}$. The limiting behavior is well defined, but resolution of the flight phase requires an $\mathcal{O}(\frac{1}{\bar{v}})$ calculation.

We note that (2.30) also shows that, as $\bar{v} \to \infty$, the sweep angle approaches the straight line $\Delta\psi = (\pi - 2\beta + 2\delta_n)$ from below, within its domain of definition; in fact, the $\mathcal{O}(\frac{1}{\bar{v}})$ correction to $\Delta\psi$ is the square root of the ratio of potential energy at midstance to kinetic energy at touchdown.

2.2. Gravitational effects during stance. We have argued that, for sufficiently stiff leg springs, elastic force dominates gravitational force during the stance phase. In this situation, their inclusion represents a small perturbation of the idealized case studied above. Order of magnitude estimates indicate that, for the mass and leg length chosen here, a relatively stiff spring (e.g., $k = 2000\frac{N}{m}$, $\gamma = 306$) is required to justify the neglect of g. Typical apex heights are one to two orders of magnitude larger than η_0 in this case. However, even with springs as soft as $k = 100\frac{N}{m}$ ($\gamma = 15.3$), chosen so that flight phase displacements are comparable to those in the stance phase, the hopper exhibits asymptotically stable gaits similar to those of the idealized case. Figure 4 shows four examples of COM trajectories in physical space. Also see Figure 2.

2.3. On pitching dynamics: $d \neq 0$. We have found numerical evidence of periodic gaits even when the leg is not attached at the COM so that the (freely pivoted) body pitches in response to the combined moments due to gravity and the leg-spring force, according to the last equation of (2.4). Figure 5 shows examples of symmetric 1:1 motions in which the pitching angle is periodic with the same (least) period as the COM translation dynamics; note that in

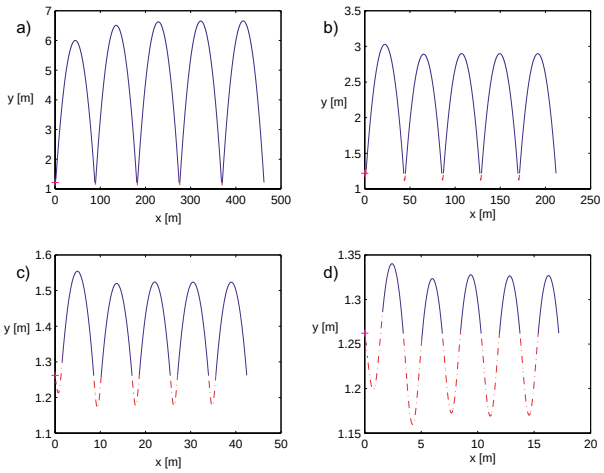

Figure 4. *Stable gaits with gravity included in the stance phase, showing the effect of spring stiffness.* $m = 1, \eta_0 = 1.5$, $k = 2000$ ($\gamma = 306$) (a); $k = 1000$ ($\gamma = 153$) (b); $k = 250$ ($\gamma = 38.2$) (c); *and* $k = 100$ ($\gamma = 15.3$) (d). *Here* $\beta = 0.95$ *for the upper graphs, and* $\beta = 1.0$ *for the lower ones.* v_n *was* $45, 35, 15, 8$, *respectively. Stance phases are shown chain dotted, and flight phases are shown solid; note the differing vertical scales.*

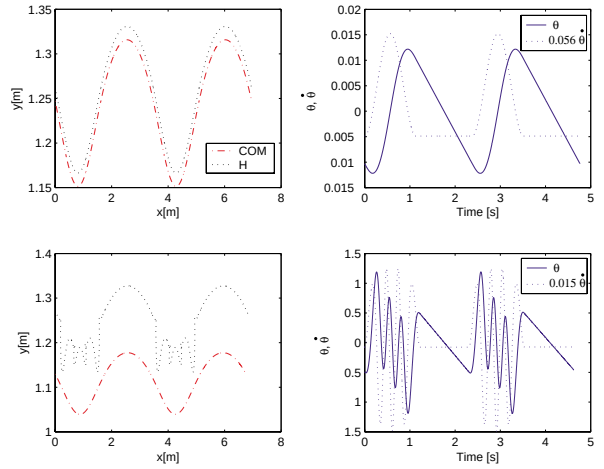

Figure 5. *Periodic gaits of the model with pitching included* ($d \neq 0$). *The left-hand panels show COM and hip paths in physical space, and the right-hand panels show pitch angle and angular velocity. Computed for parameter values* $k = 100, m = 1, \eta_0 = 1.5, \beta = 1$, *and* (a) $d = 0.015, I = 2.25 \times 10^{-2}, \bar{v} = 7.93$; (b) $d = 0.15, I = 2.25 \times 10^{-4}, \bar{v} = 8.26$. *Note that* $\dot{\theta}$ *scales differ in right-hand panels.*

(b) the pitch angle oscillates several times during each stance phase. We have also seen higher order resonances in which the pitching pattern repeats once every n strides and quasi-periodic motions in which the pitch angle remains bounded but is not precisely locked to the stride dynamics. We defer a detailed analysis of these "acrobatic" motions, which appear to include partially asymptotically stable orbits having three eigenvalues of modulus 1 and one inside the unit circle, to a future publication.

3. Two examples. In section 2.1.3, we discussed general conditions for stability, saddle-node bifurcations, period-doubling, and the appearance of a gap, and we classified the solutions in terms of $\Delta\psi_{max}$, the maximum leg angle swept during stance, assuming only that the function $\Delta\psi(v,\delta)$ has a unique maximum but without specifying any particular spring law. In the following section, we consider two specific and commonly used spring models: a linear Hooke's law spring and an air spring that mimics the compressed air strut used in certain hopping robots. Throughout this section, we employ the approximation of section 2.1, ignoring gravity during stance.

3.1. The Hooke's law spring. To further illustrate the four cases discussed in section 2.1 (Figure 3), we numerically evaluate the Poincaré map for a system with spring potential $V(\eta) = \frac{k}{2}(\eta - \eta_0)^2$ and parameters $k = 100, m = 1, \eta_0 = 1.5, \beta = 1.25$. As before, we employ increasing initial speeds $v_0 = 1.75, 3.5, 5, 6$, corresponding to cases (a) to (d), respectively; see Figure 6. A somewhat larger set of touchdown-to-touchdown Poincaré maps P_2 is shown in Figure 7, where we plot the second component $\delta_n \mapsto \delta_{n+1}$ implicit in (2.20).

Note that, as $\bar{v}$ increases, the map first intersects the identity $\delta_{n+1} = \delta_n$ at $\bar{v} = \bar{v}_{SN}$, and fixed points appear in a saddle-node bifurcation. We illustrate this in Figure 8(a) in the form of bifurcation diagrams [34], plotting $\bar{\delta}$ vs. $\bar{v}$. No qualitative changes with β are apparent; this is a general feature that will be discussed in further detail in section 4, where we also assess the effects of gravity in the stance phase. We note that the domain of attraction of the stable fixed point opens and grows following $\bar{v} = \bar{v}_{SN}$ until it is invaded by the gap; thereafter, it shrinks as $\bar{v}$ increases. Also note that the larger δ_n fixed point disappears at a finite speed $\bar{v} \approx 5.9$ due to the change of type of $\Delta\psi$ and the stance map when $\delta \to \beta$, and kinetic energy at touchdown exceeds the potential energy stored in the spring at zero length (cf. [17], and also see Figure 7).

We have also seen gaps in the domain of definition of P_2 for low velocities $\bar{v} < \bar{v}_{SN}$ (before the saddle-node), but these are of less concern since there are no sustained gaits in this range.

As noted in section 2.1.5, period-doubling bifurcations may occur as $\bar{v}$ increases, depending upon the spring potential and other parameters. Figure 9 shows an example of a period two gait born in such a bifurcation for a linear spring system.

3.2. An air spring. The four cases discussed in section 2.1.5 can also be illustrated with an air spring model. As noted above, we adopt the potential $\frac{c}{2}(\frac{1}{\eta^2} - \frac{1}{\eta_0^2})$. We compute orbits and Poincaré maps for a system with the parameters $c = 23, m = 1, \eta_0 = 1.5, \beta = 1.25$ and increasing initial speeds $v_0 = 1.75, 3.5, 5, 6$ shown as cases (a) to (d), respectively, in Figure 10; these should be compared with Figure 6. The corresponding Poincaré maps are shown in Figure 11 for comparison with Figure 7. For small values of speed $\bar{v}$, the map has no fixed points or periodic orbits, and, as for the linear spring, fixed points appear in a saddle-node bifurcation at a critical speed $\bar{v} = \bar{v}_{SN}$. Figure 8b shows a bifurcation diagram for the air spring hopper. For this spring law, which requires infinite energy and force for compression to zero length, no change of type occurs, and the upper, unstable branch of fixed points continues to arbitrarily high velocities.

3.2.1. Period-doubling and chaos. In section 2.1.5, we showed that period-doubling may occur as $\bar{v} \to \infty$. On the other hand, there is also a critical speed $\bar{v}_{GP}$ above which the return

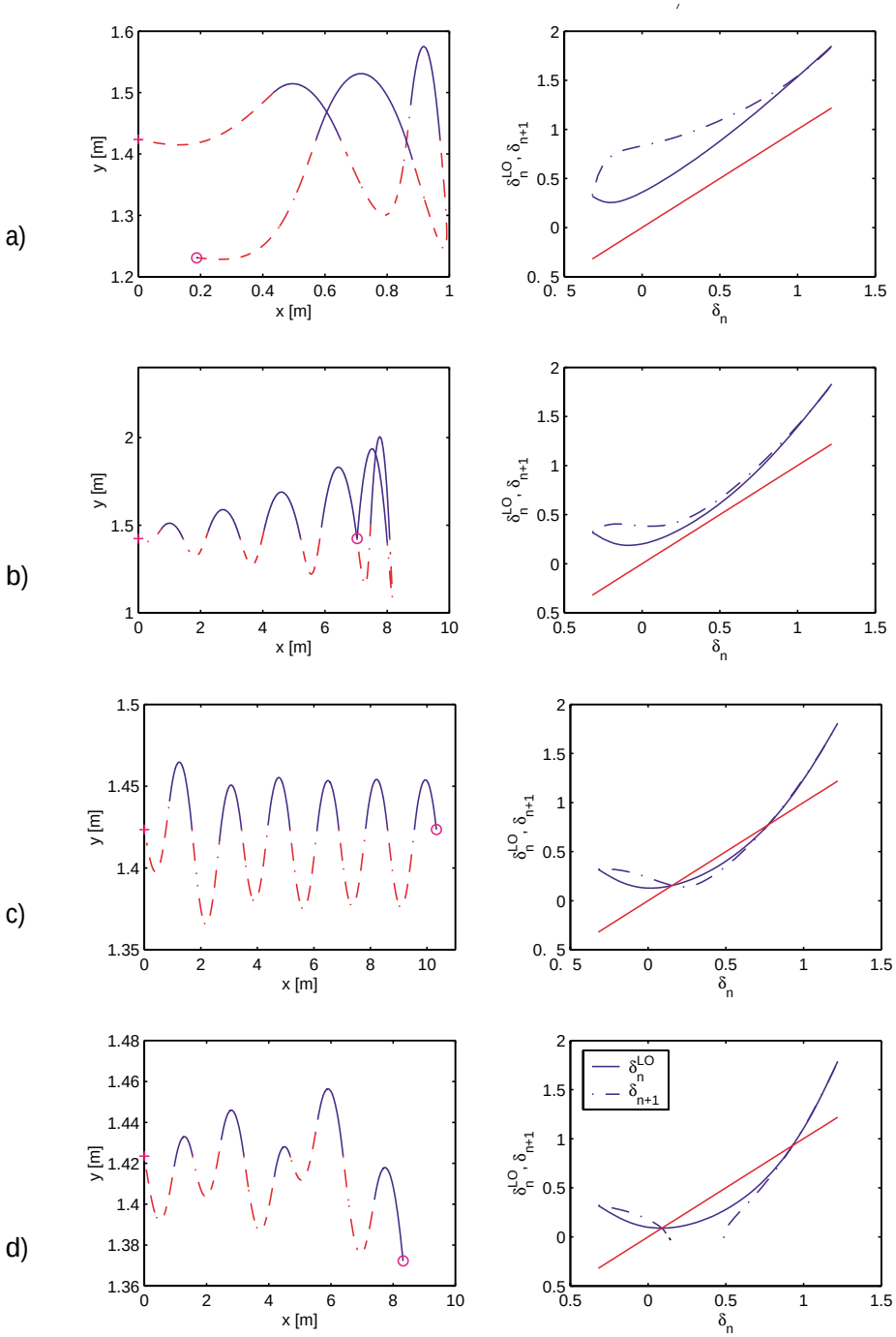

Figure 6. *Motions of the linear spring hopper in physical space (left column) and Poincaré maps (right column). Physical parameters k, m, η_0, β were taken as for Figure 3. Trajectories in physical space were computed from initial condition $\delta_0 = 0.1$, and initial speed was increased from $v_0 = 1.75$ to $3.5, 5$, and 6 for cases* (a) *to* (d), *respectively. Touchdown height is shown by dotted horizontal lines. Poincaré maps were computed for the same speeds. Fixed points occur at intersections of the curves and the line $\delta_n = \delta_{n+1}$. Both the stance map P_{st} (solid) and the full map P (dotted) are shown. In* (d), *note the gap in which the full map is not defined.*

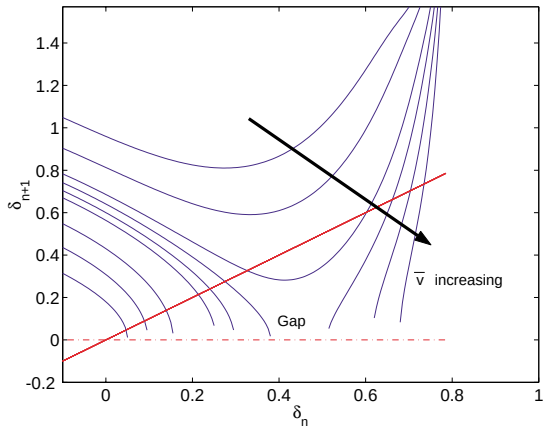

Figure 7. *The Poincaré map P_2 for a linear spring hopper with $k = 10, m = 1, \eta_0 = 1.5, \beta = \pi/4$, and speeds $\bar{v}$ ranging from 3.2 to 8. Note how the two fixed points appear in a saddle-node bifurcation, and a gap then opens as $\bar{v}$ increases. For very high speeds, only one fixed point exists.*

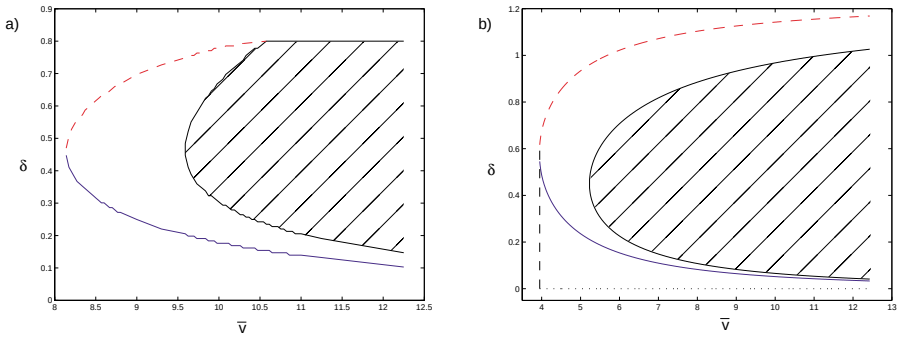

Figure 8. *Bifurcation diagrams for the linear spring hopper with $m = 1, k = 50, \eta_0 = 1.5$, and touchdown angle $\beta = 0.8$ in* (a) *and for the air spring hopper with $m = 1, c = 23, \eta_0 = 1.5$, and $\beta = 1.25$ in* (b)*. Stable branches of fixed points are shown solid, unstable branches are dashed, and cross-hatching identifies the region in which the map is not defined. Saddle-node bifurcations occur at $\bar{v}_{SN} = 8.12$ in* (a) *and $\bar{v}_{SN} = 3.95$ in* (b)*; below these no periodic gaits exist.*

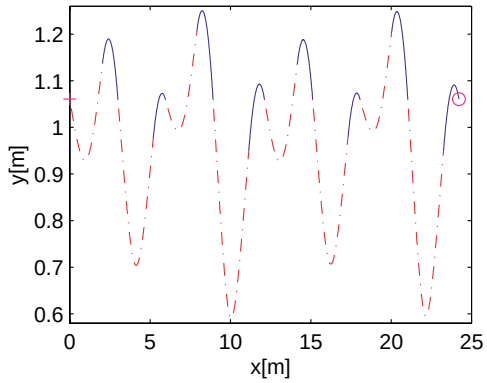

Figure 9. *A period two gait of the linear spring hopper with $k = 10, m = 1, \eta_0 = 1.5, \beta = \pi/4$, and $\bar{v} = 3.95$.*

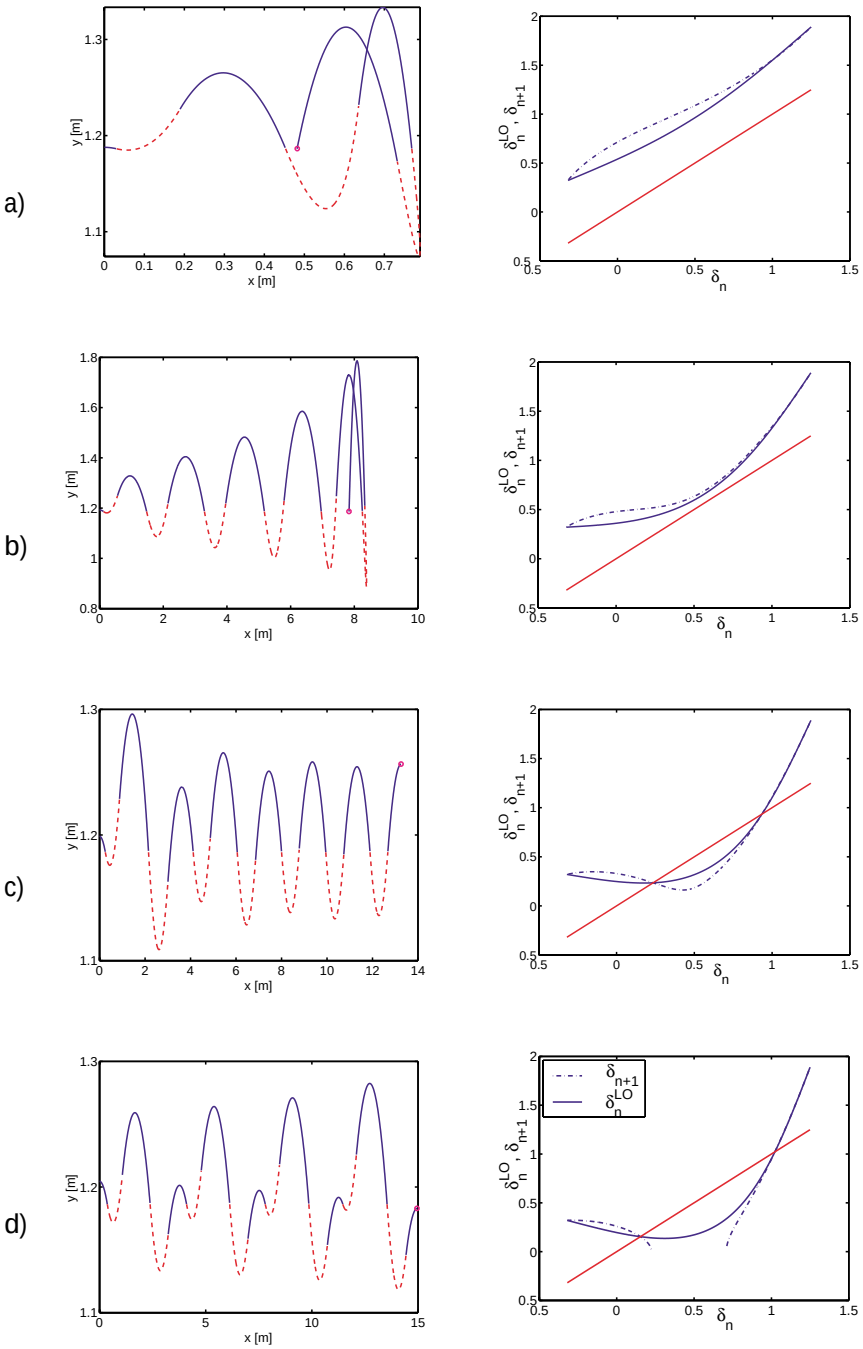

Figure 10. *Physical space motions (left column) and Poincaré maps (right column) for the air spring hopper. Parameter values were chosen as for Figure 3 except for the air spring stiffness $c = 23$ and leg length $\zeta_0 = 1.25$. The physical space trajectories were computed from initial condition $\delta_0 = 0.1$ and initial speeds from $v_0 = 1.75$ to $3.5, 5$, and 6 for cases* (a) *to* (d)*, respectively. Touchdown height is shown by dotted horizontal lines. The maps were computed for the same speeds and angles $\delta \in [0, \beta]$. Fixed points are identified with the intersection of the curves and the line $\delta_n = \delta_{n+1}$. Both the stance map P_{st} (solid) and the full map P (dash-dotted) are shown. The region in which the full map is not defined is apparent in* (d).

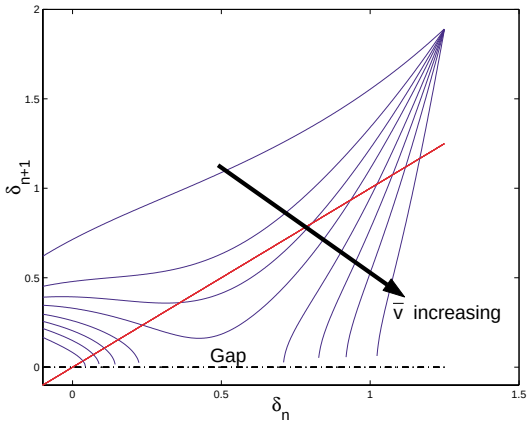

Figure 11. *The Poincaré map P_2 for an air spring hopper with $c = 23, m = 1$, and $\zeta_0 = 1.25$. The speed $\bar{v}$ ranges from 1.75 to 12.2. Note the gap and the fact that the upper (larger $\bar{\delta}$) fixed point persists.*

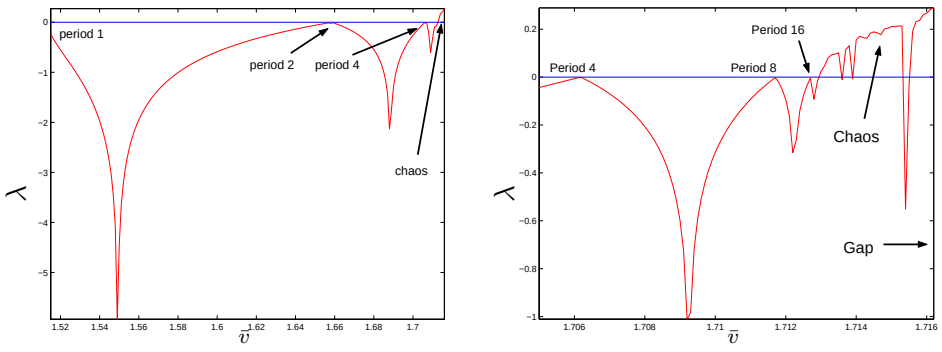

(a) (b)

Figure 12. *Lyapunov exponents for $\beta = 0.961$, $c/m = 0.01839$, $g = 9.81$, and $\eta_0 = 0.173$. The speed range where the exponent becomes positive is magnified in* (b).

map is not defined over the whole range $\delta_n \in [0, \beta]$. The question then arises whether the gap always opens *before* period-doubling occurs or whether period two and higher period orbits or even chaotic behavior is observed for gap-free return maps. This is not only of theoretical importance; the onset of higher period orbits and chaotic behavior for gap-free return maps would place additional constraints on feedforward control policies that simply keep the leg touchdown angle at $\beta = \text{const}$ [28].

To identify period-2^n orbits and chaos, we numerically approximate the Lyapunov exponent [34] λ of the one-dimensional return map $P_2 : \delta_n \mapsto \delta_{n+1}(\delta_n)$, implicitly defined by the

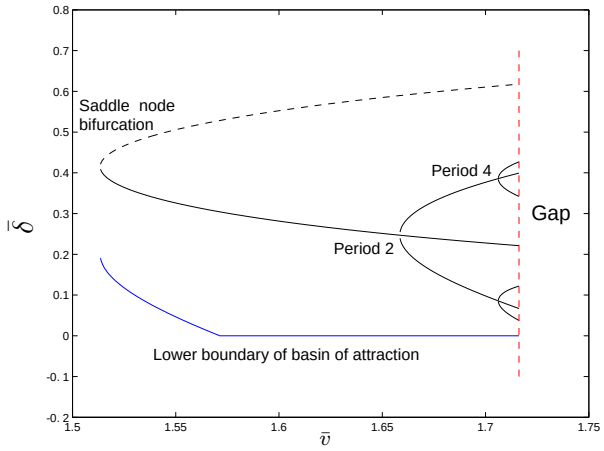

Figure 13. *Bifurcating fixed points for $\beta = 0.961$, $c/m = 0.01839$, $g = 9.81$, and $\eta_0 = 0.173$. The region between the lower blue line and the upper dashed line is the basin of attraction.*

second component of (2.20):

$$\lambda = \lim_{N\to\infty} \frac{1}{N} \sum_{i=0}^{N-1} \ln \left| \frac{dP_2}{d\delta_n}(\delta_i) \right| =: \lim_{N\to\infty} \lambda_N. \tag{3.1}$$

Specifically, we set

$$\lambda \approx \begin{cases} \lambda_K & \text{if} \quad |\lambda_K - \lambda_{K-1}| < \varepsilon \text{ and } K < \bar{N}, \\ \lambda_{\bar{N}} & \text{else} \quad (\text{with } \bar{N} = 10000 \text{ and } \varepsilon = 10^{-6}) \end{cases} \tag{3.2}$$

and take a range of leg touchdown speeds $\bar{v} \in [1.515, 7.162]$; other parameters are $\beta = 0.961$, $c/m = 0.01839$, $g = 9.81$, and $\eta_0 = 0.173$. In this case, the return map develops a gap at $\bar{v}_{GP} = 1.7162$.

However, it can be seen from Figure 12(a) that λ crosses to positive values at $\bar{v}_{Chaos} \approx 1.713$ (magnified in Figure 12(b)). Similar behavior has been observed for the air spring potential *with* gravity in stance for parameter values $\beta = 0.961$, $c/m = 0.03839$, $g = 9.81$, and $\eta_0 = 0.17$. Here, the Lyapunov exponent becomes positive at $\bar{v}_{Chaos} = 1.6932$, whereas the gap opens at $\bar{v}_{GP} = 1.697$. This is strong numerical evidence for chaotic behavior in the corresponding SLIP. Chaotic behavior has not been observed for the linear spring.

In Figure 13, the corresponding bifurcating branches of fixed points are plotted as a function of the touchdown speed $\bar{v}$ up to the gap at $\bar{v}_{GP}$. Bifurcations of period eight and higher are omitted. The lower boundary of attraction is also shown; this deviates from $\delta_n = 0$ whenever $\delta_{n+1}(0) > \delta_{n+1}(\bar{\delta}_1^{us})$, where $\bar{\delta}_1^{us}$ denotes the unstable fixed point of the period one bifurcation.

4. Nondimensional parameter studies. Parameters intrinsic to the model are the mass m of the body, the moment of inertia I, the gravitational acceleration g, the uncompressed leg length η_0, the leg touchdown angle β, the distance d from hip to the COM, and the stiffnesses k or c. These, together with initial conditions v_0, δ_0, provide a variety of solutions

with different stance and flight phases and basins of attraction. The seven physical parameters can be reduced to a minimal set of *nondimensional* parameters necessary to characterize the model. Rescaling time and lengths by defining $\tilde{t} = \frac{t}{t_0}, \tilde{\zeta} = \frac{\zeta}{\eta_0}, \tilde{d} = \frac{d}{\eta_0}$, and $\tilde{\eta} = \frac{\eta}{\eta_0}$, we can rewrite the equations of motion (2.4) as

$$\begin{aligned}
\tilde{\zeta}'' &= \psi'^2\tilde{\zeta} - \frac{gt_0^2}{\eta_0}\cos\psi - \frac{V_{\tilde{\zeta}}(\eta_0\tilde{\eta})t_0^2}{m\eta_0^2\tilde{\eta}}(\tilde{\zeta} + \tilde{d}\cos(\psi+\theta)),\\
\tilde{\zeta}\psi'' &= -2\psi'\tilde{\zeta}' + \frac{gt_0^2}{\eta_0}\sin\psi + \tilde{d}\frac{V_{\tilde{\zeta}}(\eta_0\tilde{\eta})t_0^2}{m\eta_0^2\tilde{\eta}}\sin(\psi+\theta),\\
\theta'' &= \tilde{d}\frac{V_{\tilde{\zeta}}(\eta_0\tilde{\eta})\,\tilde{\zeta}t_0^2}{I\tilde{\eta}}\sin(\psi+\theta),
\end{aligned} \tag{4.1}$$

where the differentiation $()' \equiv \frac{d}{d\tilde{t}}$ is with respect to the nondimensional time $\tilde{t}$, and $V_{\tilde{\zeta}}(\tilde{\eta}) = V_{\tilde{\eta}}(\tilde{\eta}) = \frac{\partial}{\partial\tilde{\eta}}V(\tilde{\eta})$. It seems physically reasonable to define the characteristic time $t_0 = \frac{\eta_0}{v_0}$, where v_0 is a characteristic speed, such as the COM speed at touchdown, and η_0 is the uncompressed length of the leg spring.

4.1. Hooke's law spring. If we assume a linear spring with $V(\eta_0\tilde{\eta}) = \frac{k\eta_0^2}{2}(\tilde{\eta}-1)^2$ and define the nondimensional parameter groups

$$\tilde{k} \triangleq \frac{kt_0^2}{m} = \frac{k\eta_0^2}{mv_0^2},\ \tilde{g} \triangleq \frac{gt_0^2}{\eta_0} = \frac{g\eta_0}{v_0^2},\ \text{and}\ \tilde{I} \triangleq \frac{I}{m\eta_0^2}, \tag{4.2}$$

the equations of motion, expressed in nondimensional coordinates, become

$$\begin{aligned}
\tilde{\zeta}'' &= \psi'^2\tilde{\zeta} - \tilde{g}\cos\psi - \tilde{k}\left(1-\frac{1}{\tilde{\eta}}\right)(\tilde{\zeta} + \tilde{d}\cos(\psi+\theta)),\\
\tilde{\zeta}\psi'' &= -2\psi'\tilde{\zeta}' + \tilde{g}\sin\psi + \tilde{k}\tilde{d}\left(1-\frac{1}{\tilde{\eta}}\right)\sin(\psi+\theta),\\
\theta'' &= \frac{\tilde{k}\tilde{d}\tilde{\zeta}}{\tilde{I}}\left(1-\frac{1}{\tilde{\eta}}\right)\sin(\psi+\theta).
\end{aligned} \tag{4.3}$$

Here the parameter $\tilde{k} = \frac{k\eta_0^2}{mv_0^2} = \frac{E_{spr}}{E_{kin}}$ expresses the ratio between the potential energy storable by the spring at maximum compression (i.e., to zero length) and the touchdown kinetic energy, whereas $\tilde{g} = \frac{g\eta_0}{v_0^2}$, a Froude number, expresses the ratio of gravitational energy to kinetic energy. Note also that the ratio $\frac{\tilde{k}}{\tilde{g}} = \frac{k\eta_0}{mg} \triangleq \gamma$ is fixed for a given physical system and is independent of initial conditions and, in particular, of the characteristic speed. Seven physical parameters $m, I, d, \eta_0, \beta, g, k$ have been reduced to five: $\tilde{I}, \tilde{d}, \beta, \tilde{g}, \tilde{k}$. In the special case of the hip attached at the COM $\tilde{d} = 0, \theta = \text{const}$ and only three parameters play a role: $\beta, \tilde{g}, \tilde{k}$. This facilitates a parametric analysis of the system. Since β does not appear to change the qualitative behavior of the solutions of (4.3), we represent the "sheets" of periodic solutions in $(\tilde{k}, \tilde{g}, \bar{\delta})$-space.

Since we wish to assess the influence of gravity via $\tilde{g}$, here and for the air spring calculations below, we *include* gravity in the stance phase and make our fixed-point computations numerically.

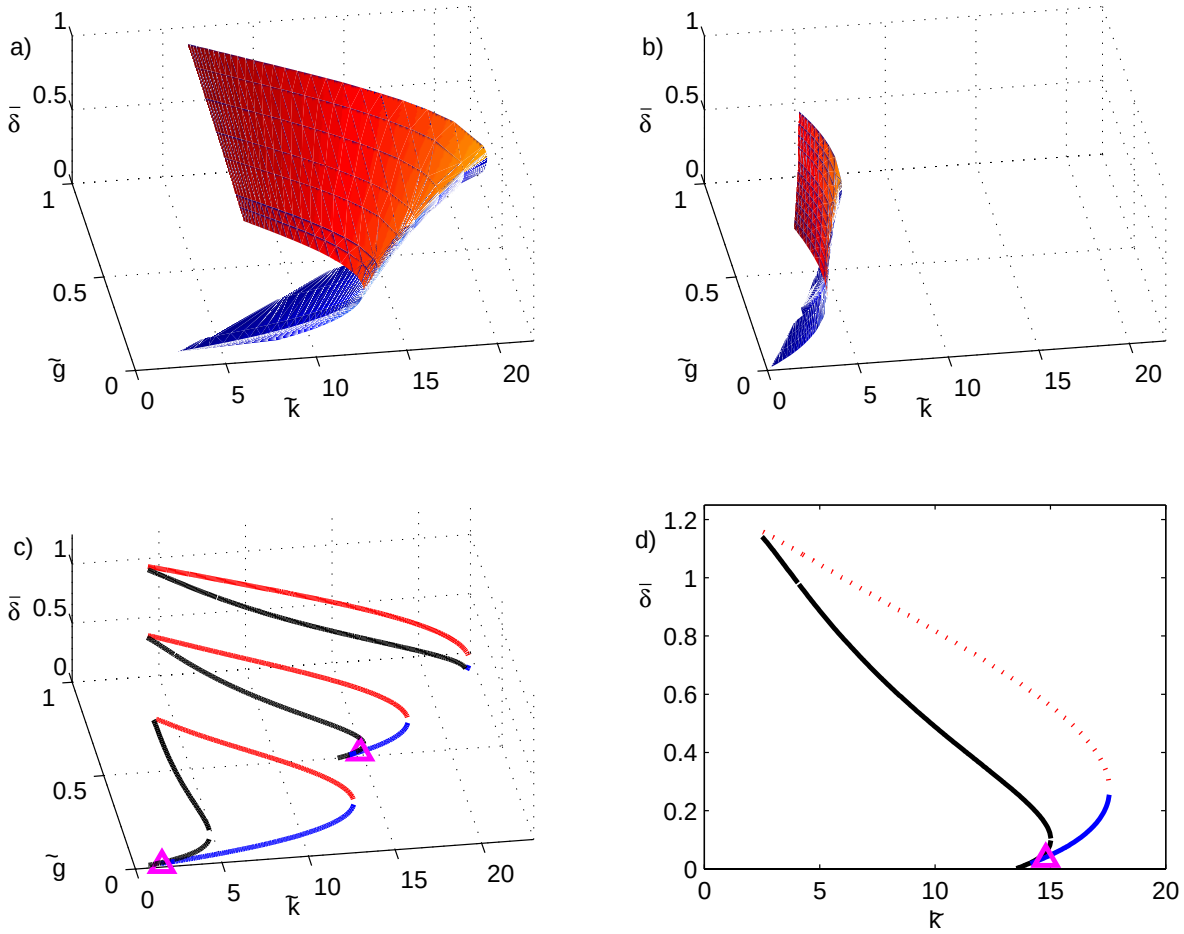

Figure 14. *Bifurcation diagrams for the linear spring in nondimensional $(\tilde{k}, \tilde{g}, \bar{\delta})$-parameter space. Upper panels show the cases $\beta = 1.25$ (a) and $\beta = 1$ (b), respectively; lower panels show three bifurcation diagrams (cross sections of* (a)*) for $\beta = 1.25$ (c) and a single bifurcation diagram for $\beta = 1.25$ and $\tilde{g} = 0.5$ (d). Unstable branches are shown dashed, stable branches are shown solid, period-doubling bifurcation points are indicated by triangles, and boundaries of the gap are indicated by thick black curves.*

Figures 14(a)–(b) show how the stable and unstable branches of the fixed point $\delta_n = \bar{\delta}$ over $(\tilde{k}, \tilde{g})$-space change as β varies. The general shape of the surface of equilibria is preserved, although the influence of $\tilde{g}$ on the saddle-node location $\tilde{k}_{SN}$ lessens as β decreases and $\tilde{k}_{SN}$ itself decreases, corresponding to higher velocities. Also, for fixed β, increases in $\tilde{g}$ cause the lower (stable) branch to shrink until it disappears so that when gravity plays a dominant role (low speed and/or long leg), there is only one *unstable* fixed point; cf. Figure 14(c) with $\tilde{g} \approx 1$. It can also happen, as noted in section 3.1 (Figure 8(a)), that the upper branch terminates and only one (potentially) stable fixed point exists, e.g., near $\beta = 1.25, \tilde{k} \approx 1, \tilde{g} \approx 0.01$ in Figure 14(c). Increasing β has the effect of expanding the domain of attraction both in the $\tilde{k}$ and $\bar{\delta}$ directions. This suggests a choice of high ratios γ (e.g., relatively hard springs) and high values of β in order to maximize the domains of attraction of the stable fixed points.

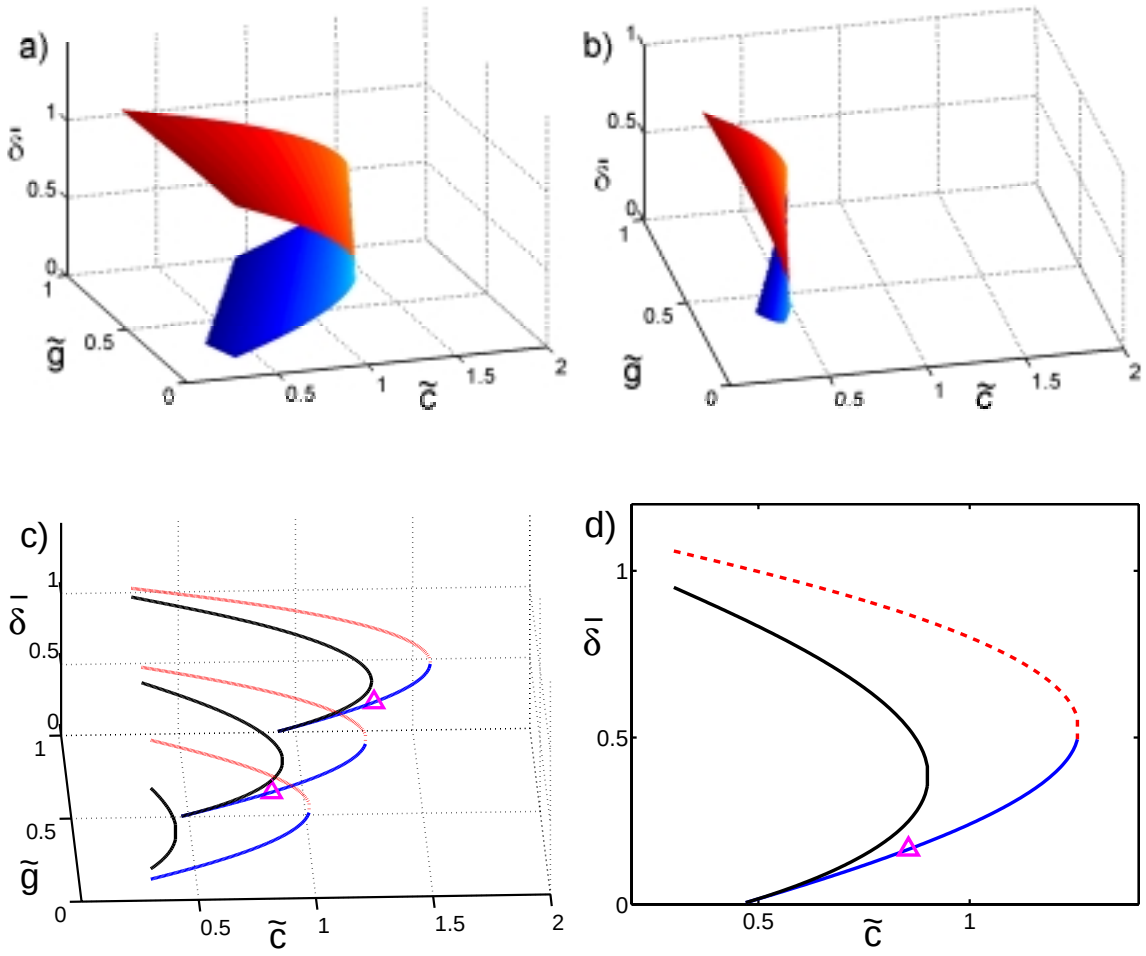

Figure 15. *Bifurcation diagrams for the air spring in nondimensional $(\tilde{c}, \tilde{g}, \bar{\delta})$-parameter space. Upper panels show the cases $\beta = 1.25$ (a) and $\beta = 1$ (b), respectively; lower panels show three bifurcation diagrams (cross sections of* (a)*) for $\beta = 1.25$ (c) and a single bifurcation diagram for $\beta = 1.25$ and $\tilde{g} = 0.5$ (d). Unstable branches are shown dashed, stable branches are shown solid, period-doubling bifurcation points are indicated by triangles, and boundaries of the gap are indicated by thick black curves.*

We note that, for fixed $(\tilde{k}, \tilde{g}, \beta)$, the saddle-node and other bifurcations occur at particular velocities $\bar{v}_{SN}$, etc. It therefore follows from (4.2) that, as k and/or m vary and other physical parameters remain fixed,

$$\bar{v}_{SN} = \eta_0 \sqrt{\frac{k}{m\tilde{k}_{SN}}} \propto \sqrt{\frac{k}{m}}. \tag{4.4}$$

This is presumably the type of scaling mentioned in [22, section 4.1]. See [19] for extensive analyses of this type for the LLS model.

4.2. Air spring. If we assume an air spring with $V(\eta_0\tilde{\eta}) = \frac{c}{2\eta_0^2}(\frac{1}{\tilde{\eta}^2} - 1)$ and define the nondimensional parameter groups

$$\tilde{c} \triangleq \frac{ct_0^2}{m\eta_0^4} = \frac{c}{mv_0^2\eta_0^2}\ ,\ \tilde{g} \triangleq \frac{gt_0^2}{\eta_0} = \frac{g\eta_0}{v_0^2},\ \text{and}\ \tilde{I} \triangleq \frac{I}{m\eta_0^2}, \tag{4.5}$$

the equations of motion, expressed in nondimensional coordinates, become

$$\begin{aligned}
\tilde{\zeta}'' &= \psi'^2\tilde{\zeta} - \tilde{g}\cos\psi + \frac{\tilde{c}}{\tilde{\eta}^4}(\tilde{\zeta} + \tilde{d}\cos(\psi+\theta)),\\
\tilde{\zeta}\psi'' &= -2\psi'\tilde{\zeta}' + \tilde{g}\sin\psi - \frac{\tilde{c}}{\tilde{\eta}^4}\tilde{d}\sin(\psi+\theta)\,,\\
\theta'' &= -\frac{\tilde{c}\tilde{d}\tilde{\zeta}}{\tilde{\eta}^4\tilde{I}}\sin(\psi+\theta)\,.
\end{aligned} \tag{4.6}$$

Note that with these choices, $\tilde{c} = \frac{c}{m\eta_0^2v_0^2} = \frac{E_{spr}}{E_{kin}}$ expresses the ratio between the potential energy stored at infinite spring length and the kinetic energy, whereas $\tilde{g} = \frac{g\eta_0}{v_0^2}$ is again the Froude number. Note also that the ratio $\frac{\tilde{c}}{\tilde{g}} = \frac{c}{mg\eta_0^3} \triangleq \mathring{\gamma}$ is fixed for a given physical system and, like γ above, is independent of initial conditions and of the characteristic speed. Again, seven physical parameters $m, I, d, \eta_0, \beta, g, c$ have been reduced to five: $\tilde{I}, \tilde{d}, \beta, \tilde{g}, \tilde{c}$. In the special case of the hip attached at the COM $\tilde{d} = 0, \theta = \text{const}$ and only three parameters play a role: $\beta, \tilde{g}, \tilde{c}$. The resulting surface plots are generally similar to those of Figure 14 for the linear spring, but they reveal that stable branches persist for large $\tilde{g}$ and that period-doubling occurs "earlier" (for higher $\tilde{c}$ and hence lower $\bar{v}$); see Figure 15.

5. Conclusions. In this paper, we studied the SLIP model of a hopping rigid body in the vertical plane. Exploring suitable limiting cases, we proved the existence of asymptotically stable periodic gaits for a fixed leg-angle (feedforward) touchdown protocol by studying the touchdown-to-touchdown Poincaré map in its exact form and under the approximation that gravity is negligible during stance. Numerical simulations including gravitational effects corroborated this result, revealing regions in the parameter and phase spaces where stable gaits exist. We considered two representative spring laws: a linear spring and a hardening air spring, and we studied bifurcations from the branch of stable gaits, the domains of attraction of those gaits, and the domains of definition of the Poincaré map, picking parameter values appropriate to illustrating key behaviors rather than for comparison with specific animals or machines. Throughout we focused on the classical SLIP, but our formulation includes full rigid body dynamics in the sagittal plane, and we displayed some coupled translation and pitching motions. Future work will include a broader analysis of these aspects.

As noted in the introduction, our work complements the study of [22], which addresses parameter ranges relevant to human running. Using direct numerical solution of the point mass SLIP equations (equivalent to the first two of (2.6)), [22] identifies parameters for which potentially stable period one gaits exist and shows that models with masses, leg lengths, and stiffnesses estimated from human data fall within a narrow range [22, Figure 2(A)]. A set of apex height Poincaré maps and some COM trajectories are also shown [22, Figures 3(A–B)].

It is noted that there is a minimum speed below which periodic gaits do not exist, that "larger variations in leg stiffness and angle of attack are tolerated [for] increasing speed," and that "higher ... velocities require either higher leg stiffness assuming constant angle of attack, or flatter angles of attack for constant leg stiffness" [22, Figures 2(B–C)].

We believe that the present analytical work, with the associated limiting integrable limiting cases, illuminates those observations. Specifically, our bifurcation studies reveal limits to stable parameter ranges bounded by saddle-node and period-doubling bifurcations, the former being responsible for [22]'s minimum speed requirement; our nondimensional analysis shows clear speed/stiffness relations (e.g., (4.4) for the linear spring) and reveals the relative importance of elastic and gravitational effects; and our study of gaps in the domain of definition of P ([22]'s apex/touchdown height constraint) shows that, while stable fixed points or higher period orbits continue to high velocity, their domains of attraction become extremely small. This shows that, with increasing speed, the system is *less* tolerant to dynamical perturbations, even though *parameter* variations are less restricted, as observed in [22] (see also Figure 2(b) in [25]). However, the bifurcation diagrams of Figures 8 and 14 show that, if the nondimensional parameters are maintained in a "good" location (e.g., between the saddle-node and gap of Figure 8) as $\bar{v}$ changes, by suitable tuning of stiffness or touchdown angle, then robust stability can be achieved with simple fixed-leg reset control. This viewpoint is guiding our development of "low attention" feedback controllers, to be described in a future paper [28].

Appendix A. Air spring sweep angle. The sweep angle $\Delta\psi\,(v_n, \delta_n)$ can be obtained explicitly in terms of elementary functions for an air spring model with $V\,(\eta) = \frac{c}{2}(\frac{1}{\eta^2} - \frac{1}{\eta_0^2})$. For $d = 0$ (hip attached to the COM), $\eta \equiv \zeta$. Solving first for the midstance compressed length using conservation of energy and angular momentum, we obtain

$$\frac{1}{2}mv_0^2 = \frac{1}{2}\frac{p_\psi^2}{m\zeta_{\min}^2} + \frac{c}{2}\left(\frac{1}{\zeta_{\min}^2} - \frac{1}{\zeta_0^2}\right) \Rightarrow \zeta_{\min} = \zeta_0\sqrt{\frac{p_\psi^2 + mc}{m^2v_n^2\zeta_0^2 + mc}}. \tag{A.1}$$

Using this in the quadrature (2.10) with $v_n = v_0$ and $p_\psi = m\zeta_0 v_0 \sin(\beta - \delta_n)$, the sweep angle may be computed as

$$\Delta\psi(v_0, \delta_n) = \frac{2p_\psi}{\sqrt{mc + p_\psi^2}} \arccos\left(\sqrt{\frac{p_\psi^2 + mc}{m^2v_0^2\zeta_0^2 + mc}}\right). \tag{A.2}$$

Finally, redefining $\tilde{c} = \frac{c}{m\zeta_0^2v_0^2}$, $z = \sin(\beta - \delta_n)$, $\hat{c} = \frac{\tilde{c}}{1+\tilde{c}}$, and $\hat{z} = \sqrt{\frac{z^2+\tilde{c}}{1+\tilde{c}}}$, $\Delta\psi$ can be rewritten as

$$\Delta\psi(v_0, \delta_n) = 2\frac{z}{\sqrt{1+\tilde{c}}}\frac{\arccos\left(\sqrt{\frac{z^2+\tilde{c}}{1+\tilde{c}}}\right)}{\sqrt{\frac{z^2+\tilde{c}}{1+\tilde{c}}}} = 2\sqrt{1 - \frac{\hat{c}}{\hat{z}^2}}\arccos(\hat{z}). \tag{A.3}$$

Appendix B. Limiting behavior as $\bar{v} \to \infty$. We recall the quadrature integral (2.10)

$$\Delta\psi = 2\eta_0 \sin(\beta - \delta_n)\int_{\zeta_b}^{\eta_0} \frac{d\zeta}{\zeta\sqrt{\zeta^2 - \frac{2\zeta^2V(\zeta)}{m\bar{v}^2} - \eta_0^2\sin^2(\beta - \delta_n)}}, \tag{B.1}$$

where ζ_b is the compressed leg length at midstance, satisfying the energy balance

$$\left[1 - \frac{2V(\zeta_b)}{m\bar{v}^2}\right]\zeta_b^2 = \eta_0^2 \sin^2(\beta - \delta_n). \tag{B.2}$$

(Note that we do not (yet) assume the fixed-point condition $\delta_n = \bar{\delta}$.) Under the standing assumption of analyticity of V in $(0, \eta_0)$, we first estimate the relevant solution of (B.2) and then examine the asymptotics of $\Delta\psi$ as $\bar{v} \to \infty$.

We introduce the small (dimensional) parameter $\epsilon = \frac{1}{\bar{v}^2}$ and expand solutions of (B.2) in the form $\zeta_b \approx \zeta_{b_0} + \epsilon\zeta_{b_1} + \cdots$, obtaining

$$\zeta_{b_0} = \eta_0 \sin(\beta - \delta_n) \ , \quad \zeta_{b_1} = \frac{\zeta_{b_0} V(\zeta_{b_0})}{m}. \tag{B.3}$$

The integral (B.1) may then be written

$$\begin{aligned} \Delta\psi &\approx 2\zeta_{b_0} \int_{\zeta_{b_0}+\epsilon\zeta_{b_1}}^{\eta_0} \frac{d\zeta}{\zeta\sqrt{\zeta^2\left(1 - 2\epsilon\frac{V(\zeta)}{m}\right) - \zeta_{b_0}^2}} \\ &\approx 2\zeta_{b_0} \int_{\zeta_{b_0}+\epsilon\zeta_{b_1}}^{\eta_0} \frac{d\zeta}{\zeta\sqrt{\zeta^2 - \zeta_{b_0}^2}} + \frac{2\epsilon\zeta_{b_0}}{m} \int_{\zeta_{b_0}+\epsilon\zeta_{b_1}}^{\eta_0} \frac{\zeta V(\zeta) d\zeta}{(\zeta^2 - \zeta_{b_0}^2)^{\frac{3}{2}}}. \end{aligned} \tag{B.4}$$

The first integral of (B.4) yields leading terms of $\mathcal{O}(1)$ and $\mathcal{O}(\sqrt{\epsilon}\,)$

$$2\left[\arccos(\sin(\beta - \delta_n)) - \arccos\left(\frac{\zeta_{b_0}}{\zeta_{b_0} + \epsilon\zeta_{b_1}}\right)\right] \approx \pi - 2\beta + 2\delta_n - 2\sqrt{\frac{2\epsilon\zeta_{b_1}}{\zeta_{b_0}}}, \tag{B.5}$$

where the $\mathcal{O}(\sqrt{\epsilon}\,)$ term is computed by setting $\arccos\left(\frac{\zeta_{b_0}}{\zeta_{b_0}+\epsilon\zeta_{b_1}}\right) \approx k_0 + \epsilon^\alpha k_1$ and solving for k_0, k_1, and α.

Integrating the second term of (B.4) twice by parts, we obtain

$$\begin{aligned} &\frac{2\epsilon\zeta_{b_0}}{m}\left(\left[\frac{-V(\zeta)}{\sqrt{\zeta^2 - \zeta_{b_0}^2}} + V'(\zeta)\ln\left(\zeta + \sqrt{\zeta^2 - \zeta_{b_0}^2}\right)\right]\Bigg|_{\zeta_{b_0}+\epsilon\zeta_{b_1}}^{\eta_0}\right. \\ &\qquad \left. - \int_{\zeta_{b_0}+\epsilon\zeta_{b_1}}^{\eta_0} V''(\zeta)\ln\left(\zeta + \sqrt{\zeta^2 - \zeta_{b_0}^2}\right) d\zeta\right). \end{aligned} \tag{B.6}$$

The upper limit of the first term and both logarithmic boundary terms give contributions of $\mathcal{O}(\epsilon)$. Successive integrations by parts of the third term produce a convergent series [42], so it is also of $\mathcal{O}(\epsilon)$. To obtain the dominant $\mathcal{O}(\sqrt{\epsilon}\,)$ contribution, we therefore need only include the lower limit of the first term:

$$\frac{2\epsilon\zeta_{b_0}}{m}\frac{V(\zeta_{b_0} + \epsilon\zeta_{b_1})}{\sqrt{2\epsilon\zeta_{b_0}\zeta_{b_1} + \epsilon^2\zeta_{b_1}^2}} \approx \sqrt{\frac{2\epsilon\zeta_{b_0}}{\zeta_{b_1}}}\,\frac{V(\zeta_{b_0})}{m}. \tag{B.7}$$

Combining (B.5) and (B.7) and using (B.3), we therefore obtain

$$\Delta\psi = (\pi - 2\beta + 2\delta_n) - \sqrt{\frac{2\epsilon\zeta_{b_1}}{\zeta_{b_0}}} + \mathcal{O}(\epsilon). \tag{B.8}$$

We note that $\Delta\psi \to (\pi - 2\beta + 2\delta_n)$ from below as $\epsilon \to 0$. Substituting the expressions (B.3) once more, (B.8) yields (2.30).

The fixed-point condition $\delta_n = \bar{\delta}$ requires that $\Delta\psi\left(\bar{\delta}, v_n\right) = \pi - 2\beta$, implying

$$\bar{\delta} \approx \sqrt{\frac{\epsilon\zeta_{b_1}}{2\zeta_{b_0}}} = \sqrt{\frac{\epsilon V(\zeta_{b_0})}{2m}}. \tag{B.9}$$

Now (B.9) defines $\bar{\delta}$ only implicitly since $\zeta_{b_0} = \eta_0 \sin(\beta - \bar{\delta})$, but setting $\zeta_{b_0} \approx \eta_0 \left(\sin\beta - \bar{\delta}\cos\beta\right)$ for $\bar{\delta} = \mathcal{O}(\sqrt{\epsilon})$ and expanding $V(\zeta_{b_0}) \approx V(\eta_0 \sin\beta) - V'(\eta_0 \sin\beta)\bar{\delta}\cos\beta$, we obtain

$$\bar{\delta} = \sqrt{\frac{V(\eta_0 \sin\beta)}{2m\bar{v}^2}} + \mathcal{O}\left(\frac{1}{\bar{v}^2}\right). \tag{B.10}$$

Thus $\bar{\delta} \to 0^+$ *linearly* with $\frac{1}{\bar{v}}$ as $\bar{v} \to \infty$. We use this in (2.31).

Appendix C. Asymptotic behavior of λ_2. We recall that the second eigenvalue of the stride-to-stride map is given by

$$\lambda_2 = 1 - \left(1 + g\eta_0 \cos\beta \frac{\cot\bar{\delta}}{\bar{v}^2}\right) \left.\frac{\partial\Delta\psi}{\partial\delta_n}\right|_{f.p.}. \tag{C.1}$$

Evaluating the derivative of the sweep angle at the fixed point $(\bar{v}, \bar{\delta})$ using the expressions developed in Appendix B, and noting that $\bar{\delta} \sim \sqrt{\epsilon} = \frac{1}{\bar{v}}$, we obtain

$$\frac{\partial\Delta\psi}{\partial\delta_n} = 2 + \frac{\eta_0 \cos\beta\, V'(\eta_0 \sin\beta)}{\bar{v}\sqrt{2mV(\eta_0 \sin\beta)}} + \mathcal{O}\left(\frac{1}{\bar{v}^2}\right). \tag{C.2}$$

Then using $\cot\bar{\delta} \approx \frac{1}{\bar{\delta}} \propto \bar{v}$ and substituting (C.2) into (C.1) yield the expression (2.29):

$$\lambda_2 = -1 - \frac{\eta_0 \cos\beta\,[4mg + V'(\eta_0 \sin\beta)]}{\bar{v}\sqrt{2mV(\eta_0 \sin\beta)}} + \mathcal{O}\left(\frac{1}{\bar{v}^2}\right). \tag{C.3}$$

REFERENCES

[1] J. Nishii, *Legged insects select the optimal pattern based on the energetic cost*, Biological Cybernetics, 83 (2000), pp. 435–442.

[2] R. Full, D. R. Stokes, A. Ahn, and R. K. Josephson, *Energy absorption during running by leg muscles in a cockroach*, J. Experimental Biology, 201 (1998), pp. 997–1012.

[3] K. G. Pearson, *Central programming and reflex control of walking in the cockroach*, J. Experimental Biology, 56 (1972), pp. 173–193.

[4] M. Ahmadi and M. Buehler, *Stable control of a simulated one-legged running robot with hip and leg compliance*, IEEE Trans. Robotics Automation, 13 (1997), pp. 96–104.

[5] J. K. Hodgkins and M. H. Raibert, *Adjusting step length for rough terrain locomotion*, IEEE Trans. Robotics Automation, 7 (1991), pp. 289–298.
[6] G. M. Nelson and R. D. Quinn, *Posture Control*, IEEE Control Systems Magazine 19 (1999), pp. 9–14.
[7] R. Full and D. E. Koditschek, *Templates and anchors: Neuromechanical hypothesis of legged locomotion on land*, J. Experimental Biology, 83 (1999), pp. 3325–3332.
[8] R. Blickhan and R. Full, *Similarity in multilegged locomotion: Bouncing like a monopode*, J. Comp. Physiol. A, 173 (1993), pp. 509–517.
[9] M. H. Dickinson, C. T. Farley, R. J. Full, M. A. R. Koehl, R. Kram, and S. Lehman, *How animals move: An integrative view*, Science, 288 (2000), pp. 100–106.
[10] R. Altendorfer, N. Moore, H. Komsuoğlu, M. Buehler, H. B. Brown, Jr., D. McMordie, U. Saranli, R. Full, and D. E. Koditschek, *RHex: A biologically inspired hexapod runner*, Autonomous Robots, 11 (2001), pp. 207–213.
[11] T. McGeer, *Passive bipedal running*, Proc. Roy. Soc. London B, 240 (1990), pp. 107–134.
[12] M. Garcia, A. Chatterjee, A. Ruina, and M. J. Coleman, *The simplest walking model: Stability, complexity and scaling*, ASME J. Biomech. Engrg., 120 (1998), pp. 281–288.
[13] M. J. Coleman and A. Ruina, *An uncontrolled walking toy that cannot stand still*, Phys. Rev. Lett., 80 (1998), pp. 3658–3661.
[14] K. D. Mombaur, R. W. Longman, H. G. Bock, and J. P. Schlöder, *Stable one-legged hopping without feedback and with a point foot*, in Proceedings of the 2002 IEEE International Conference on Robotics and Automation, Vol. 4, Washington, DC, 2002, pp. 3978–3983.
[15] E. Celaya and J. M. Porta, *A control structure for the locomotion of a legged robot on difficult terrain*, IEEE Robotics and Automation Magazine, 5 (1998), pp. 43–51.
[16] T. Kubow and R. Full, *The role of the mechanical system in control: A hypothesis of self-stabilization in hexapedal runners*, Phil. Trans. Roy. Soc. London Ser. B Biol. Sci., 354 (1999), pp. 849–861.
[17] J. Schmitt and P. Holmes, *Mechanical models for insect locomotion: Dynamics and stability in the horizontal plane* I. *Theory*, Biological Cybernetics, 83 (2000), pp. 501–515.
[18] J. Schmitt and P. Holmes, *Mechanical models for insect locomotion: Dynamics and stability in the horizontal plane* II. *Application*, Biological Cybernetics, 83 (2000), pp. 517–527.
[19] J. Schmitt and P. Holmes, *Mechanical models for insect locomotion: Stability and parameter studies*, Phys. D, 156 (2001), pp. 139–168.
[20] J. Schmitt, M. Garcia, R. Razo, P. Holmes, and R. J. Full, *Dynamics and stability of legged locomotion in the horizontal plane: A test case using insects*, Biological Cybernetics, 86 (2002), pp. 343–353.
[21] D. L. Jindrich and R. J. Full, *Dynamic stabilization of rapid hexapedal locomotion*, J. Exp. Biol., 205 (2002), pp. 2803–2823.
[22] A. Seyfarth, H. Geyer, M. Günther, and R. Blickhan, *A movement criterion for running*, J. Biomechanics, 35 (2002), pp. 649–655.
[23] A. Ruina, *Non-holonomic stability aspects of piecewise holonomic systems*, Rep. Math. Phys., 42 (1998), pp. 91–100.
[24] U. Saranli, M. Buehler, and D. E. Koditschek, *RHex: A simple and highly mobile hexapod robot*, Internat. J. Robotics Research, 20 (2001), pp. 616–631.
[25] R. Altendorfer, R. M. Ghigliazza, P. Holmes, and D. E. Koditschek, *Exploiting passive stability for hierarchical control*, in Proceedings of the Fifth International Conference on Climbing and Walking Robots (CLAWAR 2002), Professional Engineering Publishing Limited, London, 2002, pp. 177–184.
[26] A. Seyfarth and H. Geyer, *Natural control of spring-like running—optimized self-stabilization*, in Proceedings of the Fifth International Conference on Climbing and Walking Robots (CLAWAR 2002), Professional Engineering Publishing Limited, London, 2002, pp. 81–85.
[27] R. Altendorfer, D. E. Koditschek, and P. Holmes, *Towards a Factored Analysis of Legged Locomotion Models*, Technical report, CSE-TR-467-02, University of Michigan, Ann Arbor, MI, 2002; to appear in Proceedings of the IEEE Automation Conference, Taipei, Taiwan, 2003.
[28] R. Altendorfer, R. M. Ghigliazza, P. Holmes, and D. E. Koditschek, *Hopping on a springy leg: "Low attention" feedback control*, manuscript.
[29] F. Gubina, H. Hemami, and R. B. McGhee, *On the dynamic stability of biped locomotion*, IEEE Trans. Biomedical Engrg., 21 (1974), pp. 102–108.

[30] M. H. Raibert, *Legged Robots that Balance*, MIT Press, Cambridge, MA, 1986.
[31] H. Goldstein, *Classical Mechanics*, 2nd ed., Addison–Wesley, Reading, MA, 1980.
[32] W. J. Schwind and D. E. Koditschek, *Approximating the stance map of a* 2 *DOF monoped runner*, J. Nonlinear Sci., 10 (2000), pp. 533–568.
[33] V. I. Arnold, *Mathematical Methods of Classical Mechanics*, Springer-Verlag, New York, 1978.
[34] J. Guckenheimer and P. Holmes, *Nonlinear Oscillations, Dynamical Systems, and Bifurcations of Vector Fields*, Springer-Verlag, New York, 1990.
[35] C. T. Farley and O. González, *Leg stiffness and stride frequency in human running*, J. Biomechanics, 29 (1995), pp. 181–186.
[36] W. J. Schwind, *Spring Loaded Inverted Pendulum Running: A Plant Model*, Ph.D. thesis, University of Michigan, Ann Arbor, MI, 1998.
[37] U. Saranli, W. J. Schwind, and D. E. Koditschek, *Toward the control of a multi-jointed, monoped runner*, in Proceedings of the IEEE International Conference on Robotics and Automation, Leuven, Belgium, 1998, pp. 2676–2682.
[38] W. J. Schwind and D. E. Koditschek, *Characterization of monoped equilibrium gaits*, in Proceedings of the IEEE International Conference on Robotics and Automation, Albuquerque, NM, 1997, pp. 1986–1992.
[39] R. L. Devaney, *An Introduction to Chaotic Dynamical Systems*, Benjamin/Cummings, Menlo Park, CA, 1986.
[40] M. J. Coleman and P. Holmes, *Motions and stability of a piecewise holonomic system: The discrete Chaplygin sleigh*, Regul. Chaotic Dyn., 4 (1999), pp. 55–77.
[41] J. I. Neimark and N. A. Fufaev, *Dynamics of Nonholonomic Systems,* Transl. Math. Monogr., 33, AMS, Providence, RI, 1972.
[42] C. M. Bender and S. A. Orszag, *Advanced Mathematical Methods for Scientists and Engineers*, McGraw–Hill, New York, 1978.